Phage Display Library Screening For Psa-/Lo Prostate Cancer Cell-Binding Peptides

John R. Moore

PHAGE DISPLAY LIBRARY SCREENING FOR PSA$^{-/lo}$ PROSTATE CANCER CELL-BINDING PEPTIDES

by

John Robert Moore, B.S.

APPROVED:

_____

Supervisory Professor: Dean Tang, M.D., Ph.D.

_____

David Johnson, Ph.D.

_____

Donna Kusewitt, D.V.M, A.C.V.P, Ph.D.

_____

Taiping Chen, Ph.D.

_____

Mark McArthur, D.V.M, A.C.V.P.

APPROVED:

_____

Dean, The University of Texas
Graduate School of Biomedical Sciences at Houston

PHAGE DISPLAY LIBRARY SCREENING FOR PSA$^{-/lo}$ PROSTATE CANCER CELL-BINDING PEPTIDES

A

THESIS

Presented to the Faculty of

The University of Texas

Health Science of Biomedical Sciences

in Partial Fulfillment

of the Requirements

for the Degree of

MASTER OF SCIENCE

by

John Robert Moore, B.S.

Houston, Texas

May, 2014

DEDICATION

To my family, whom I love and will always rely on

To my parents, for their endless love, support and encouragement

ACKNOWLEDGMENTS

Finally, I want to thank my committee members Dr. David Johnson, Dr. Donna Kusewitt, Dr. Taiping Chen and Dr. Mark McArthur. Their insight and advice have been invaluable. I also just wish to express my gratitude to everyone in Science Park, a place much more like family than like co-workers.

PHAGE DISPLAY LIBRARY SCREENING FOR PSA$^{-/lo}$ PROSTATE CANCER CELL-BINDING PEPTIDES

John Robert Moore, B.S.

Supervisor: Dean G. Tang, Ph.D.

Prostate cancer (PCa) is one of the leading malignancies affecting men worldwide. Our lab focuses on understanding the molecular mechanisms underlying prostate carcinogenesis and developing therapeutics that target the cells responsible for driving PCa and mediating therapy resistance. My master thesis research employs a phage display library screening technology aiming to identify peptides that preferentially home in to undifferentiated PCa cells, which our lab has previously demonstrated to be intrinsically resistant to castration.

There is now evidence that a population of cells in PCa possesses characteristics associated with stem cells; these cells are referred to as cancer stem cells (CSCs). CSCs have been implicated in tumor propagation, progression and recurrence. In PCa, androgen deprivation therapy (ADT) is the mainstay treatment however, the majority of patients relapse after treatments, resulting in castration-resistant prostate cancer (CRPC). Our lab has provided evidence that the phenotypically undifferentiated PCa cell population expressing low levels or no prostate specific antigen (i.e., PSA$^{-/lo}$) is enriched in prostate cancer stem cells (PCSCs) that can long-term propagate tumors and also resist ADT. The PSA$^{-/lo}$ PCa cell population represents the best characterized PCSCs and likely a cell-of-origin for CRPC. Consequently, it is important to find therapeutics that can preferentially target these

cells. To this end, we employed highly purified PSA$^{-/lo}$ LNCaP PCa cells to perform phage display library screening. Our preliminary efforts identified two peptides, JRM1 and JRM2 that displayed preferential binding to PSA$^{-/lo}$ PCa cells.

We first identified a potential peptide that may home in to the PSA$^{-/lo}$ LNCaP cells by conducting a phage display library screening of LNCaP PSA-GFP utilizing a competitive assay technique. This peptide, TEWDYLTV, referred to as JRM1, showed slight but not statistically significant, preferential binding to the PSA$^{-/lo}$ LNCaP cells. With this knowledge we carried out another phage display library screening using adherent LNCaP PSA-GFP cells and an indirect subtraction assay. The results led to the identification of peptide JRM2, GFYVGQR, which demonstrated preferential and statistically significant binding to the PSA$^{-/lo}$ LNCaP cells. With this peptide we would like to attach either anti-cancer drugs or pro-apoptotic peptides to it and measure their effectiveness at killing undifferentiated and castration-resistant PCa cells.

TABLE OF CONTENTS

LIST OF FIGURES

LIST OF TABLES

ABBREVIATIONS

nM   nanomolar

ml   milliliter

ADT   androgen-deprivation therapy

AMC   aminocoumarin

AML   acute myeloid leukemia

AP   anterior prostate

AR   androgen receptor

ASC   adipose stromal cell

ARE   androgen response elements

ATCC   American Type Culture Collection

BLAST   Basic Local Alignment Search Tool

BSA   bovine serum albumin

CARN   castration resistant Nkx3-1 expressing

CDSS   charcoal dextran-stripped serum

CML   chronic myelogeneous leukemia

CRPC   castration resistant prostate cancer

CSC   cancer stem cells

DAPI	4',6-diamidino-2-phenylindole
DLP	dorsal and lateral prostate
DP	dorsal prostate
FACS	fluorescence-activated cell sorting
FBS	fetal bovine serum
GEM	genetically engineered mouse
GS	Gleason
HSC	hematopoietic stem cell
HUVEC	human umbilical vein endothelial cells
IHC	immunohistochemical
JRM0	VEYDSWML
JRM1	TEWDYLTV
JRM2	GFYVGQR
K/T	kanamycin and tetracycline
LB	luria broth
LGPIN	low grade prostatic intraepithelial neoplasia
LP	lateral prostate
LR	Lassamine Rhodamine

LSC	Lin$^-$Sca-1$^+$CD49$^+$
MOI	multiplicity of infection
NOD/SCID	nonobese diabetic/severe combined immunodeficiency mice
PAP	prostatic acid phosphatase
PBS	phosphate buffer solution
PCR	polymerase chain reaction
PCSC	prostate cancer stem cell
PCa	prostate cancer
PEG	polyethylene glycol
PFA	paraformaldehyde
PIN	prostatic intraepithelial neoplasia
PSA	prostate specific antigen
PSAP	prostate specific antigen promoter
PSC	prostatic stem cell
PTEN	phosphate and tensin homolog deleted on chromosome 10
PTX	paclitaxel
RPM	rounds per minute
RPMI	Roswell Park Memorial Institute (medium)

RT	room temperature
SCs	stem cells
SOI	surgical orthotopic injection
TRAMP	transgenic adenocarcinoma mouse prostate
TU	transforming units
UGS	urogenital sinus
VP	ventral prostate
15-LOX2	15-lipoxygenase-2

Chapter I

Introduction

A quarter of all deaths in the United States are due to cancer. In males, prostate cancer (PCa) is estimated to have ~233,000 new cases in 2014, and of those ~29,480 will result in death [1]. In the past decades, progress has been made in the treatment and detection of PCa. The underlying mechanisms of how PCa develops and why after treatment it can relapse and metastasize remain incompletely understood [2].There is evidence involving a subset of cancer cells that can drive tumor formation and progression and facilitate metastasis and also recurrence; these cells are operationally referred to as cancer stem cells (CSCs) [3,4,5]. The CSC model has led to new understanding into cancer cell heterogeneity, and it also has the potential to lead to new therapeutics that target these cells.

1.1 Human and mouse prostate

The prostate is located at the base of the bladder and surrounds the urethra. At birth, it weighs only a few grams but by 20 years of age it weighs approximately 20 grams [6]. Some examples of prostate functions include, first through its muscle mass, helping control urine output and secretion of seminal fluid during ejaculation [7]. As an exocrine gland, it contributes to the seminal plasma, which contains a wide variety of molecules and enzymes that help in fertility and also assist in coagulation [7]. In addition, it produces prostatic fluid that reduces the acidity in the urethra, and protects the sperm [7]. Finally, as an endocrine gland, it influences both the hypothalamic and hypophyseal functions by rapidly metabolizing testosterone to dihydrotestosterone [7].

The human prostate is divided into the following three zonal structures: peripheral, central, and transition zones [8,9,10]. The largest, making up approximately 70%, is the peripheral zone where it is thought most PCa originates from (Fig. 1-1). The mouse prostate, unlike the human counterpart, is comprised of four lobes: anterior (AP), dorsal (DP), lateral

(LP), and ventral (VP) lobes (Fig. 1-1). Gene expression profiling studies suggest that the dorsal/lateral lobes of the mouse prostate are similar to the peripheral zone of the human prostate [11].
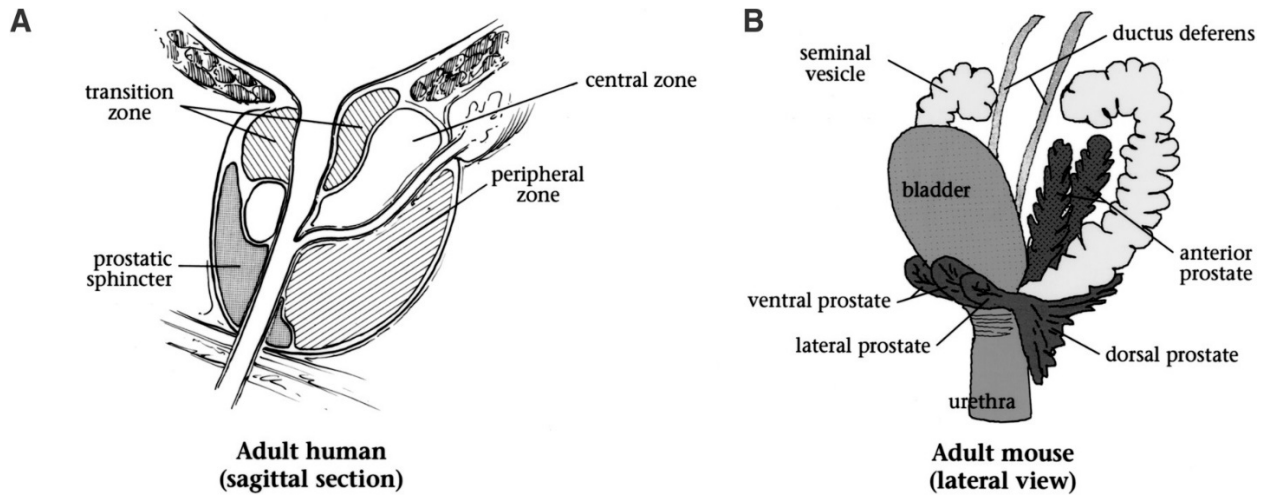
Figure 1-1. Illustrations of the anatomy of the human (A) and mouse (B) prostate.
Taken from [C. Abate-Shen, M.M. Shen. (2000) Molecular genetics of prostate cancer.
Genes Dev 14: 2410-2434.] with permission from Cold Spring Harbor Laboratory Press.

1.2 Histology of the normal prostate

Three different cell types make up the human and the mouse prostate: neuroendocrine, basal, and luminal cells [2,12,13]. Of the three cell types, neuroendocrine cells are the rarest and are distributed throughout the basal layer. Neuroendocrine cells express chromogranin A and synaptophaysin, and the functions of these cells are not well understood [2,12,13]. Basal cells are located in the basal layer, which sits on top of the basement membrane. Basal cells express p63, CK5, CK14 [14], CD44 [15], CD133, BCL-2, GST-π, telomerase, and express low to no androgen receptor (AR) protein. Luminal cells are located in the luminal layer, which sits on top of the basal cell layer. Luminal cells produce the prostate secretions and express CD57 [15], CK8, CK18, CK19, prostatic acid phosphatase (PAP), prostate specific antigen (PSA), 15-lipoxygenase-2 (15-LOX2) [16] and high levels of AR protein.

1.3 Prostate stem cells

In multicellular organisms, there is a continual turnover of cells, which requires new cells to be generated to maintain homeostasis. Old/senescent cells in organisms are eliminated through different pathways that include apoptosis and shedding from the epidermal and epithelial surfaces, and then are replaced by new cells. These new cells are provided by stem cells (SCs), which reside in specific niches in each organ. In humans, these stem cells give rise to over 200 different types of cells and possess certain characteristics such as residence in specific niches, quiescence, ability to self-renew, and the ability to generate multiple different cell types [17].

There are two different populations of cells that could harbor mouse prostatic stem cells (PSCs), basal cells or luminal cells. Upon castration/androgen deprivation, the prostate

regresses with ~90% of the luminal cells and a small number of basal cells undergoing apoptosis [18]. Upon androgen re-administration, the luminal cell layer is regenerated, presumably from, surviving basal cells [18]. This evidence suggests that PSCs may reside within the basal cell layer. Using the tissue recombination assay, multiple studies have provided evidence that basal cells are enriched in PSCs. When basal cells from the proximal prostatic glands are isolated and then sorted into Sca-1$^+$/Sca-1$^-$ cell populations, the Sca-1$^+$ cells exhibit the capacity to regenerate prostate like tissue when implanted under the renal capsules compared to the Sca-1$^-$ cells [19]. In addition, ~60% of the Sca-1$^+$ cells are also positive for α6 integrin (CD49f) and Bcl-2 [19]. Further studies have shown that Lin$^-$Sca-1$^+$CD49f$^+$ (LSC) also reside in the basal layer of the proximal region, and these cells have a 60 fold enrichment for colony and sphere formation compared to their negative counterparts. *In vivo*, these cells have tissue-regeneration capabilities, and within the regenerated tissues contain cells with both luminal and basal markers [20]. Later studies reveal that Trop2^{hi} LSC cells are even further enriched with PSC [21]. In yet another study, a single Lin$^-$Sca-1$^+$CD133$^+$CD44$^+$CD117$^+$ murine prostatic cell localized in the basal layer is capable of regenerating prostatic-like tissue that contain cells positive for basal, luminal, and neuroendocrine markers [22].

There also exists evidence that PSCs are located in the luminal cell compartment. For example, the urogenital sinus (UGS) from p63$^{-/-}$ (p63 is a basal cell marker) mouse embryos, when implanted under the renal capsule, regenerated prostatic tissues containing luminal and neuroendocrine cells but not basal cells, suggesting that p63$^{-/-}$ UGS epithelial cells, i.e., luminal cells, possess bipotent differentiation capability [23]. A lineage tracing study in castrated mouse prostates revealed a small population of luminal cells that express

Nkx3.1, referred to as CARNs (castration resistant Nkx3-1 expressing) and possess long-term self-renewal potential [24]. In tissue reconstitution assays, CARNs are capable, as single cells, of regenerating prostatic tissue [24]. Another lineage tracing study with mice subjected to prostatic regression-restoration showed that the basal cells only gave rise to CK5 positive basal cells whereas luminal cells only gave rise to CK8 positive luminal cells [25]. Interestingly, luminal cells seemed to be more sensitive to malignant transformation when crossed to a $PTEN^{-/-}$ mouse model, as compared to basal cells, which needed to differentiate into luminal cells before they could be oncogenically transformed by the loss of PTEN [25]. These results indicate that both basal and luminal compartments in the mouse prostate have a subset of PSCs that can maintain each cell linage independently.

To directly study human prostate stem cells, linage-tracing strategies cannot be applied. Therefore, most studies rely on FACS-based purification of candidate cell populations followed by tissue regeneration assays in mice. The majority of such studies indicate that human PSCs reside in the basal compartment. One such study shows that basal cells isolated from benign human prostatic tissue that express high levels of α2β1 integrin possess SC characteristics based on clonogenic and prostate duct-regeneration assays [26]. A follow-up study from the same group demonstrates that human PSCs in the basal layer express high levels of both α2β1 and CD133 and that such $α2β1^{hi}CD133^{+}$ cells have higher proliferative and prostate duct regenerating capacity than the $α2β1^{hi}CD133^{-}$ cells [27]. These studies indicate that human PSCs may reside in the basal compartment but does not rule out the possibility that the luminal compartment may also harbor SCs

1.4 PCa development and treatment

PCa generally develops very slowly, taking many years to go from a normal prostate to prostatic intraepithelial neoplasia (PIN), early and late stage carcinoma, and finally metastasis and castration resistant prostate cancer (CRPC) [2]. Adenocarcinomas are cancers of epithelial tissues that have glandular functions. In PCa, more than 95% of PCa are classified as adenocarcinomas. Adenocarcinomas in the prostate are marked by the increase in luminal like cells that express luminal markers such as CK18, AR, and PSA, and very few basal like cells that express basal marker such as p63, CK5, and CK14. This correlates with the evidence that androgen and androgen receptor (AR) signaling play important functions in PCa development [2,28]. Another key aspect of PCa is the dysregulation of many key genes. In the early onset of PCa, it is common to have down-regulation of *NKX3.1*, overexpression of *MYC,* and oncogenic gene fusions between *TMPRESS2* and *ERG*. As PCa progresses, *PTEN* is frequently inactivated and *ERK/MAPK* often activated. In advanced PCa and CRPC, *EZH2* overexpression is frequently observed [2]. The oncogenic gene fusion between TMPRESS2 and ERG is the most common genomic rearrangement in PCa, occurring in ~50% of cases [29,30]. Many mechanisms have been proposed for the development of CRPC; however, most center on AR signaling [2,28].

PCa treatment depends on when the cancer is first diagnosed. If it is detected at an early stage, the most common treatment is a radical prostatectomy, and with this treatment the prognosis is good. If PCa is diagnosed at a late stage, the main treatment is androgen-deprivation therapy (ADT). Two new drugs used in ADT are abiraterone and MDV3100 (Enzalutamide). Arbiraterone stops androgen synthesis whereas MDV3100 is an anti-androgen that blocks androgen receptor (AR) functions. ADT is effective at de-bulking the

primary tumor but most of the treated patients re-lapse and develop CRPC [31,32]. CRPC is aggressive and metastasizes to bone, lung, and liver, which makes treatment less effective (Fig. 1-2). The cell-of-origin of CRPC is unclear and therapies that target this population need to be developed.
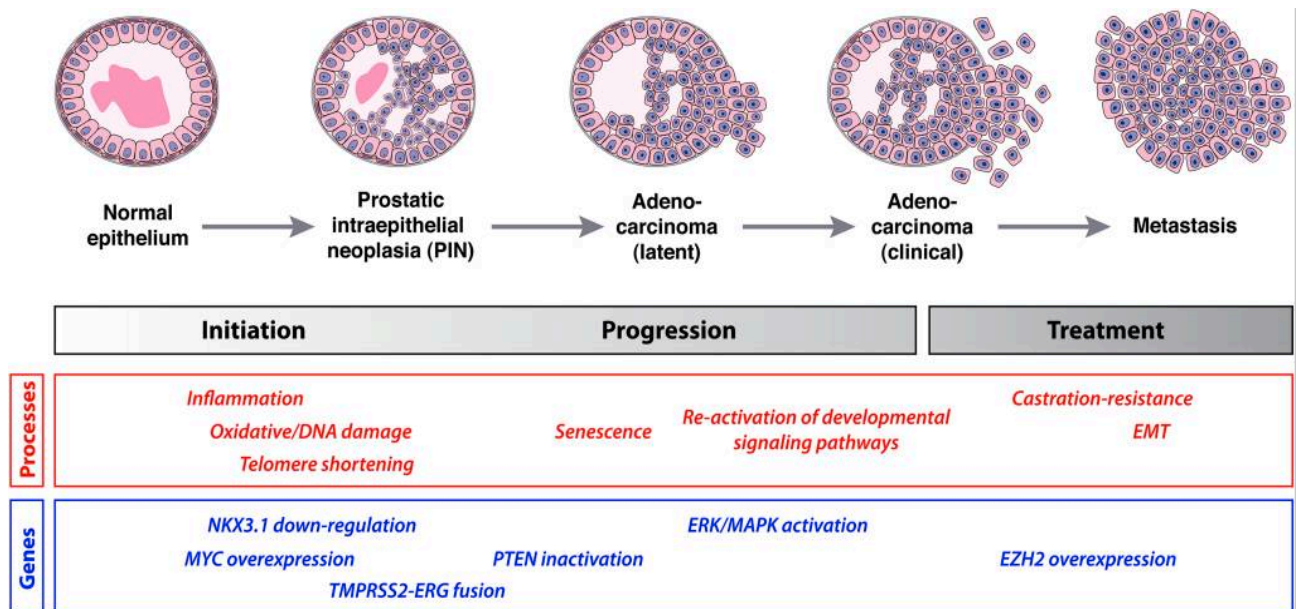
Figure 1-2. Progression of human PCa. The stages of PCa progression are shown, along with the molecular processes and genes that are likely involved at each stage. Taken from [M.M. Shen, C. Abate-Shen. (2010) Molecular genetics of prostate cancer: new prospects for old challenges. Genes Dev 24: 1967-2000.]with permission from Cold Spring Harbor Laboratory Press.

1.5 Cancer cell heterogeneity

Most cancers including PCa are heterogeneous, containing cells that are both phenotypically and functionally unique from one another [5]. Two models have been put forth to account for cancer cell heterogeneity: clonal evolution and the cancer stem cell (CSC) model. The clonal evolution model, first proposed in the 1970's by Nowell, predicts that tumor initiation and progression are an evolutionary process driven by stepwise, somatic-cell mutations with sequential, sub-clonal selection [33]. The first evidence supporting this model was established in cytogenetic studies of chronic myelogeneous leukemia (CML), which revealed a translocation between chromosomes 9 and 22 (Philadelphia chromosome), indicating that human tumors were derived from individual clones of cells with genetic abnormalities [34]. Blast phase CML is linked to additional cytogenetic alterations in leukemic cells [33].

In contrast to the clonal evolution model, the CSC model, also referred to as the hierarchical model, proposes that only a biologically distinct subset of cancer cells, i.e, CSCs, is responsible for and capable of maintaining tumor progression within the total tumor cell population, and thus establishing the heterogeneity of the tumor. CSCs possess characteristics that are associated with normal SC's, including the ability to give rise to all cell types in a tumor and to self-renew. Recent evidence argues that the clonal evolution and CSC models are not mutually exclusive and may interweave to generate tumor cell heterogeneity [5,35] (Fig. 1-3).
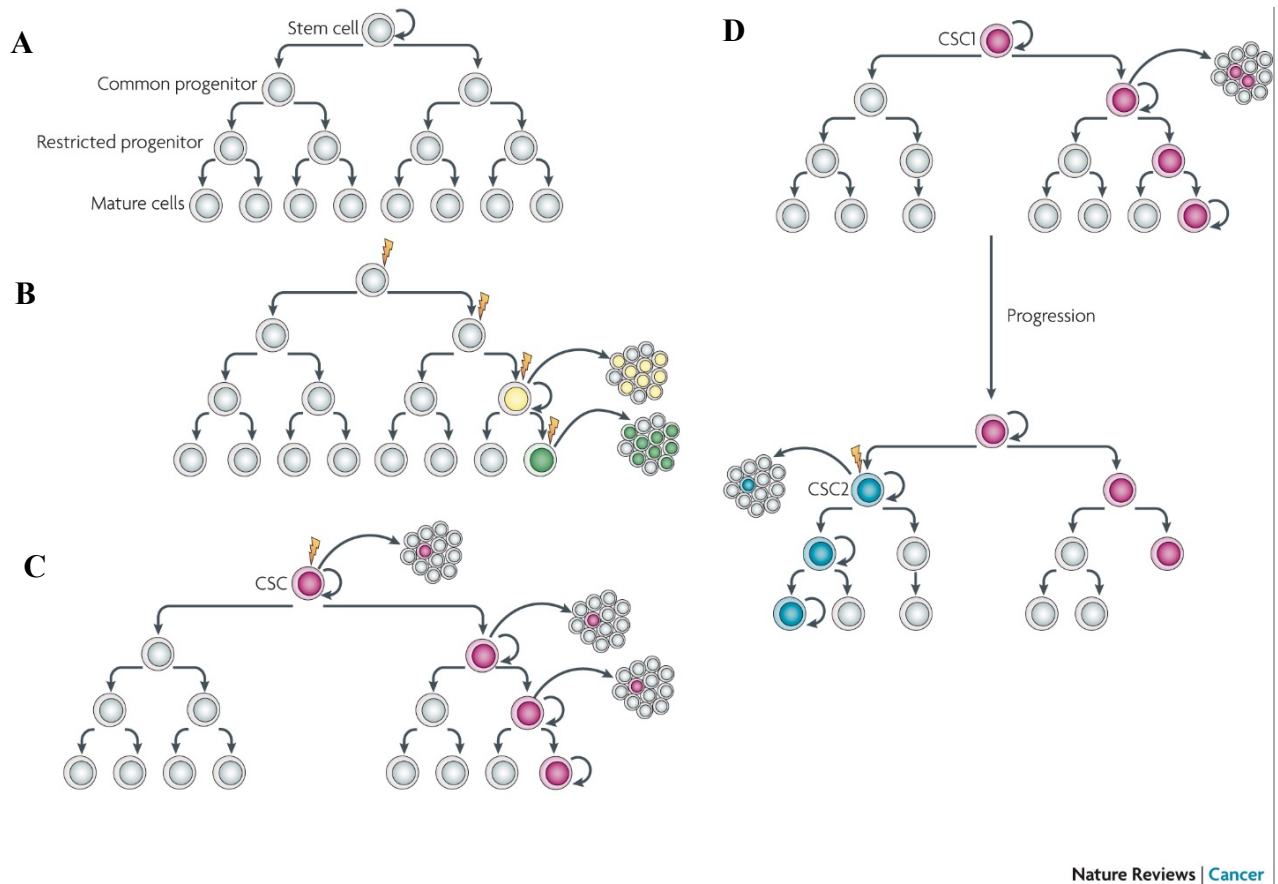
Figure 1-3. Two models for tumor heterogeneity and how they could work together. **A.** normal cellular hierarchy comprising stem cells (at the apex), which progressively generate common and more restricted progenitor cells, ultimately yielding all the mature cell types that constitute a particular tissue. **B.** In the clonal evolution model all undifferentiated cells have similar tumorigenic capacity. **C.** In the cancer stem cell (CSC) model, only the CSC can generate a tumour, based on its self-renewal properties and enormous proliferative potential. **D.** Both models of tumour maintenance may underlie tumorigenesis. Initially, tumour growth will be driven by a specific CSC (CSC1). With tumour progression, another distinct CSC (CSC2) may arise due to clonal evolution of CSC1. This may result from the acquisition of an additional mutation or epigenetic modification. This more aggressive CSC2 becomes dominant and drives tumour formation.Taken with permission from [J.E. Visvader, G.J. Lindeman. (2008) Cancer stem cells in solid tumours: accumulating evidence and unresolved questions. Nat Rev Cancer 8: 755-768.]

.

1.6 Evidence and identification of CSCs

The first evidence that suggested a CSC model came in 1937 with a study that showed that a single murine leukemic cell had the ability to regenerate a tumor in a mouse [36]. The first definitive evidence of CSCs came from John Dick's lab in the 1990s, when it was found that a small subset of AML (acute myeloid leukemia) cells bearing the normal HSC (hematopoietic stem cell) phenotypic markers (CD34$^+$CD38$^-$), when implanted into the immunodeficient (NOD/SCID) mice, could serially transplant human AML [37,38]. In 2003, another critical report provided the first evidence for CSCs in a solid tumor. Breast cancer cells with the phenotypic markers CD44$^+$CD24$^{-/lo}$ could generate tumors at as few as 100 cells in NOD/SCID mice. The regenerated tumors were serially transplantable, with the corresponding CD44$^-$CD24$^+$ cell population being much less tumorigenic [39]. Since 2003, CSCs have been widely studied in leukemia [40,41,42,43] as well as in multiple solid tumors including those in the breast [44,45,46], colon [47,48], brain [49,50,51], bladder [52,53], lung [54,55], ovary [56,57] and prostate [12,58,59,60,61,62].

CSCs are defined by their ability to self-renew and differentiate into many cell types in a tumor. Experimentally, putative CSCs can be studied by purification using fluorescence-activated cell sorting (FACS) with cell surface markers [37,38,39]. Once purified, one *in vitro* study is to plate sorted cells and test their serial sphere-formation capabilities. *In vivo*, the FACS-sorted cell populations can be implanted into immunodeficient mice to compare the tumorigenic potential of different populations. In the mean time, experiments can be performed to determine whether the regenerated tumors can be serially transplanted, and whether the regenerated tumors resemble the parental tumor. These studies are insightful but have some inherent pitfalls. Many of these PCa studies utilize long-term cultured cell lines

13

such as LNCaP, VCaP, Du145, and PC-3, derived from advanced or metastatic tumors. PCa progresses slowly through different stages from PIN, early adenocarcinoma and advanced adenocarcinoma, and finally to metastasis and CRPC. Using these cell lines does not allow us to study these different stages of PCa development. Another issue in using cultured cell lines is that they lack cell-cell and cell-stroma interactions such as the interactions between basal, neuroendocrine, and stromal cells. If utilizing xenograft transplantation models with human cell lines, the regenerated tumors often do not resemble the histology of the patient tumors and such experiments require the use of immunodeficient mice that lack a fully functioning immune system, which is a critical component in cancer progression and metastasis. For these reasons, the development of genetically engineered mice are critical for understanding the progression, compartmental interactions, and developing effective therapeutics.

1.7 Promoters used in genetically engineered mouse models of prostate cancer

The characterization of the transcriptional regulatory elements of genes, expressed in the prostate, allowed for the development of genetically engineered mouse (GEM) models. The promoter region of the rat C3(1) gene, which encodes for a subunit of prostatic binding protein secreted by the rat's ventral prostate, could direct transgene expression to the prostatic epithelial cells of mice, although the transgene expression is also evident in the seminal vesicles, testes, salivary glands, and the thyroid [63,64,65,66,67] (Table. 1-1). The next advance came when a small (-426 bp to +28 bp) rat probasin DNA segment that contain two androgen receptor response elements (ARE) was utilized [68]. The level of expression of the transgene in the mouse prostate is relatively low and is not completely restricted to the prostate as some expression is seen in the seminal vesicles [68]. To overcome the low

prostate expression a larger (-11.5 kb to +28bp) rat probasin gene promoter is used. The transgene expression driven by this promoter in the mouse prostate is higher, but the transgene is still expressed in the seminal vesicles [69]. Finally, to bypass the need of this large construct a new probasin promoter was designed by fusing the small rat probasin promoter (-426 bp to +28bp) with a segment of its enhancer region that contains two ARE's. This promoter, known as ARR_2PB, has a high transgenic expression in the mouse prostatic epithelium. It is most highly expressed in DLP (dorsal and lateral prostate) followed by the anterior prostate, and it is also highly regulated by androgens [70,71] (Table. 1-1). When characterizing a genetically engineered mouse model, it is essential to understand the promoter being used. A few aspects of a promoter to be considered are the tissue or tissues it is expressed in and the level of transgene expression (Table 1-1).

Table 1-1. Transcriptional regulatory elements used to drive transgene expression in the mouse prostate*

Promoter	Expression	Ectopic expression
Rat C3(1)	VP > DP	Seminal vesicles, testis, thyroid, salivary gland, cartilage
426 bp to +28 bp rat probasin	VP > DLP, AP (starts before puberty)	Seminal vesicles
11.5 kb to +28 bp rat probasin	VP > LP > DP > AP (starts before puberty)	Seminal vesicles
ARR2PB	VP, DLP > AP (starts in newborn mice)	Prostate stroma, seminal vesicles, testis
6 kb PSA	LP > DP > VP, AP (starts at puberty)	None reported

*Adapted and used with permission from [M. Parisotto, D. Metzger. (2013) Genetically engineered mouse models of prostate cancer. Mol Oncol 7: 190-205.]
.

1.8 Commonly utilized GEM models of prostate cancer

A few GEM models used in the research of PCa shall be discussed below. The TRAMP (transgenic adenocarcinoma mouse prostate) model utilizes the -426 bp to +28bp rat probasin promoter to drive the expression of the SV40 early region [68]. TRAMP mice express the T-antigen oncoprotein in the dorsal, lateral, and ventral prostates. When maintained in C57BL/6 background, 100% of male mice exhibit PINs between 2-3 months of age, which then progress to neuroendocrine carcinoma by 4-7 months [72,73]. By 4-9 months metastases are present primarily in the lungs and lymph nodes but appear on occasion in the kidney, liver and adrenal glands (Table 1-1). One major disadvantage in these mice is that they develop neuroendocrine carcinoma, which is rare in human PCa.

The transcription factor c-Myc is known to be overexpressed or amplified in PCa, and it regulates cellular proliferation and apoptosis [74,75,76,77,78]. Three different probasin promoters were used to overexpress c-Myc: C3(1)-c-Myc, ARR$_2$PB-Myc, and probasin-Myc [66,79]. First, overexpression utilizing the C3(1) promoter induced low grade prostatic intraepithelial neoplasia (LGPIN)s in the ventral prostate, which did not progress further. These mice lost reproductive function after five generations, which was most likely caused by transgene expression in the reproductive tissues [66]. When comparing Pb-Myc to the ARR$_2$PB-Myc transgenic models, both expressed c-Myc in the prostate as early as 2 weeks, but the Pb-Myc mice had higher expression levels [79]. In both models, PIN lesions appeared at 2 weeks and then progressed to adenocarcinomas by 3-6 months of age, with all lesions occurring in the VP, DP, LP, and, to a lesser extent, in the AP [79]. Both Pb-Myc and ARR$_2$PB-Myc PCa models develop adenocarcinomas without overt metastasis.

The development of knock-out mice is useful because it mimics what happens in human cancers [80]. PTEN (phosphate and tensin homolog deleted on chromosome 10) gene, which encodes a lipid phosphatase that dampens Akt activity, is one of the most commonly deleted genes in PCa. Bi-allelic ablation of PTEN is embryonically lethal, but the heterozygous mutant (PTEN$^{+/-}$) is viable and develops neoplasia in multiple tissues, which include lymphoid cells, adrenal glands, mammary glands, thyroid, intestines, and endometrium [81,82,83,84]. Most of the heterozygous mutants die of lymphomegaly and splenomegaly by 8 months, but the ones that do survive exhibit PINs by 8-10 months that do not progress to adenocarcinoma (Table 1-2).

Crossing the PTEN $^{+/-}$ mice with other tumor suppressor mutant mice enhances tumorigenesis. The Ink4a/Arf locus encodes two different tumor suppressors p16INK4a and p19ARF, which regulate pRB and p53 pathways, respectively. The Pten$^{+/-}$/Ink4a/Arf$^{+/-}$ mice develop PINs at a younger age compared to the Pten$^{+/-}$ mice alone [85] (Table 1-2). The Pandolfi group showed that Pten inactivation induces cell cycle arrest through p53 dependent cellular senescence pathway. When Pten$^{+/-}$ mouse model is crossed with Trp53 mouse model the Pten$^{+/-}$/Trp53$^{-/-}$ mice exhibit invasive PCa as early as 2 weeks, which becomes lethal by 7 months [86].

Throughout my stay in the Tang lab as well as my Master's thesis research, I have been involved in a GEMM project that investigates the potential tumor-suppressive functions of 15-Lipooxygenase 2 or 15-LOX2. 15-LOX2 is a human prostate specific lipid-peroxidizing enzyme, which is down-regulated or completely lost in >70% of PCa cases. Our lab has provided evidence that 15-LOX2 functions as a tumor suppressor. In a recent study, we attempted to determine whether 15-LOX2 possesses *in vivo* anti-tumor properties

by crossing 15-LOX2 transgenic animals, generated in our lab [87] with PCa-prone Hi-Myc mouse model. Both mouse models utilize the ARR2Pb promoter to drive expression of their transgenes. Strikingly, the double transgenic mice showed a significant reduction in PIN and PCa prevalent in age-matched Hi-Myc prostates. The double transgenic prostates also showed an increase in cell senescence and expression of several senescence-associated molecules including p27, phosphorylated Rb, and Rb1cc1. This part of the work has recently been accepted for publication [Cell Cycle, 2014, in press]. Since the 15-LOX2 related work that I have been involved in [2010 Oncogene; 2014 Cell Cycle] is not part of my master thesis research project, I shall not present it herein.

Table 1-2. Examples of prostate cancer GEMM.*

Mouse line	HGPIN latency	Invasive tumors (latency)	Incidence of metastasis	Site of metastasis	Latency of metastasis
TRAMP	3 months	Neuroendocrine carcinoma (4-7 months)	~100%	Lymph node, lung, adrenal gland, bone	4-9 months
ARR2PB-c-Myc	<3 months	Adenocarcinoma (3-6 months)	0%	NA	NA
PTEN$^{+/-}$	8-10 months	None	0%	NA	NA
PTEN$^{+/-}$/ Nkx3.1$^{-/-}$	>6 months	(> 6 months)	25%	Lymph node	>1 year
PB-Cre4/ PTEN$^{L2/L2}$	6-9 weeks	Adenocarcinoma (3 months)	50%	Lymph node, lung	3 months
PB-Cre4/Trp53$^{L2/L2}$ /Rb$^{L2/L2}$	Not reported	Adenocarcinoma; neuroendocrine differentiation. (< 6 months)	70%	Lymph node, liver, lung, adrenal gland	<7 months
PB-Cre4/PTEN$^{L2/L2}$ /SMAD4$^{L2/L2}$	>2 months	Adenocarcinoma (< 3 months)	100%	Lymph node and lung	<8 months
PB-Cre4/PTEN$^{L2/L2}$ /Trp53$^{L2/L2}$/SMAD4$^{L2/L2}$	<4 months	(< 4 months)	> 10%	Bone metastasis	<4 months
PSA-Cre-ERT2 /PTEN$^{L2/L2}$	8-10 months	Adenocarcinoma (14-16 months)	0%	NA	NA

*Adapted and used with permission from [M. Parisotto, D. Metzger. (2013) Genetically engineered mouse models of prostate cancer. Mol Oncol 7: 190-205.]
.

Chapter II

Phage Display Technique

2.1 Basic phage display technique

Phage display, first described in 1985 by George P. Smith [88], is a technique that allows polypeptides with desired properties to be obtained from large libraries of variants. To construct these libraries, the main method used is site directed mutagenesis, which involves the replacing of unique codons with codons that are able to encode for all twenty natural amino acid, from the phage coat protein gene segment. Each phage will then possess a unique inserted DNA sequence in the phage coat protein gene and will display a unique polypeptide on the surface of the phage. This provides a link between phenotype and genotype [89] and allows additional rounds of selection to be carried out. Phage display screening utilizes the M13 filamentous phage, which possesses a circular single-stranded DNA enclosed in a long protein capsid cylinder (Fig. 2-1). This bacteriophage is specific for Escherichia coli (K91), and does not kill the bacteria but uses the K91 host for its replication.

The basic phage display cycle has seven steps (Fig. 2-2). The first step is to obtain a bacteriophage library that consists of 10^6-10^{11} different bacteriophages with each bacteriophage displaying a unique peptide on the selected phage coat protein. The most commonly used phage coat protein is the PIII coat protein. The second step is to incubate the target cells with the bacteriophage library. This allows the peptides displayed on the phage coat protein to attach to the cells. In the third step, excess bacteriophages that do not attach are washed off. In the fourth step, the bacteriophage that have attached to the cells are eluted. The fifth step is to amplify the eluted bacteriophages. The host K91 bacteria are kanamycin resistant, and when the bacteriophages infect the bacteria, it imparts tetracycline resistance. The tetracycline resistance allows for selection of only the bacteria that have

been infected to form colonies on plates that have kanamycin and tetracycline in them. The sixth step is to titrate the bacteriophages using serial dilutions on kanamycin and tetracycline plates and then stock the bacteriophage library for future rounds of purification. Then, 2-3 more rounds of similar infection, elution, selection, and purification cycles will be carried out. Finally, single bacteria colonies from kanamycin and tetracycline plates are collected and genomic DNA sequenced using primers that are specific to either side of the unique DNA insert on the PIII (phage coat protein) gene [90]. This will provide the coding sequence of the peptide displayed on the bacteriophage (Fig. 2-1). One key aspect of phage display is that the initial library may contain 10^6-10^{10} different peptides displayed on bacteriophages, but as more rounds of purification are completed, each consecutive round will contain a less diverse library. The affinity of the peptides for the target cells in that library will increase but the phage diversity will decrease (Fig. 2-3). It is therefore important that the initial round should contain a wide range of peptides so that by the time of sequencing there are still some peptides to work with.

Figure 2-1. Diagram of the M13 phage and its genome. The M13 bacteriophage genome is composed of 5 coat protein genes (III, VI, VII, VIII, and IX), 3 genes associated with assembly/export (I, IV, and IX) and 3 genes for replication (II, V, and X) [w.w.N.a.C. Inc, Molecular Biology of Viruses, in: S. Foster (Ed.), Microbiology, 2010.]
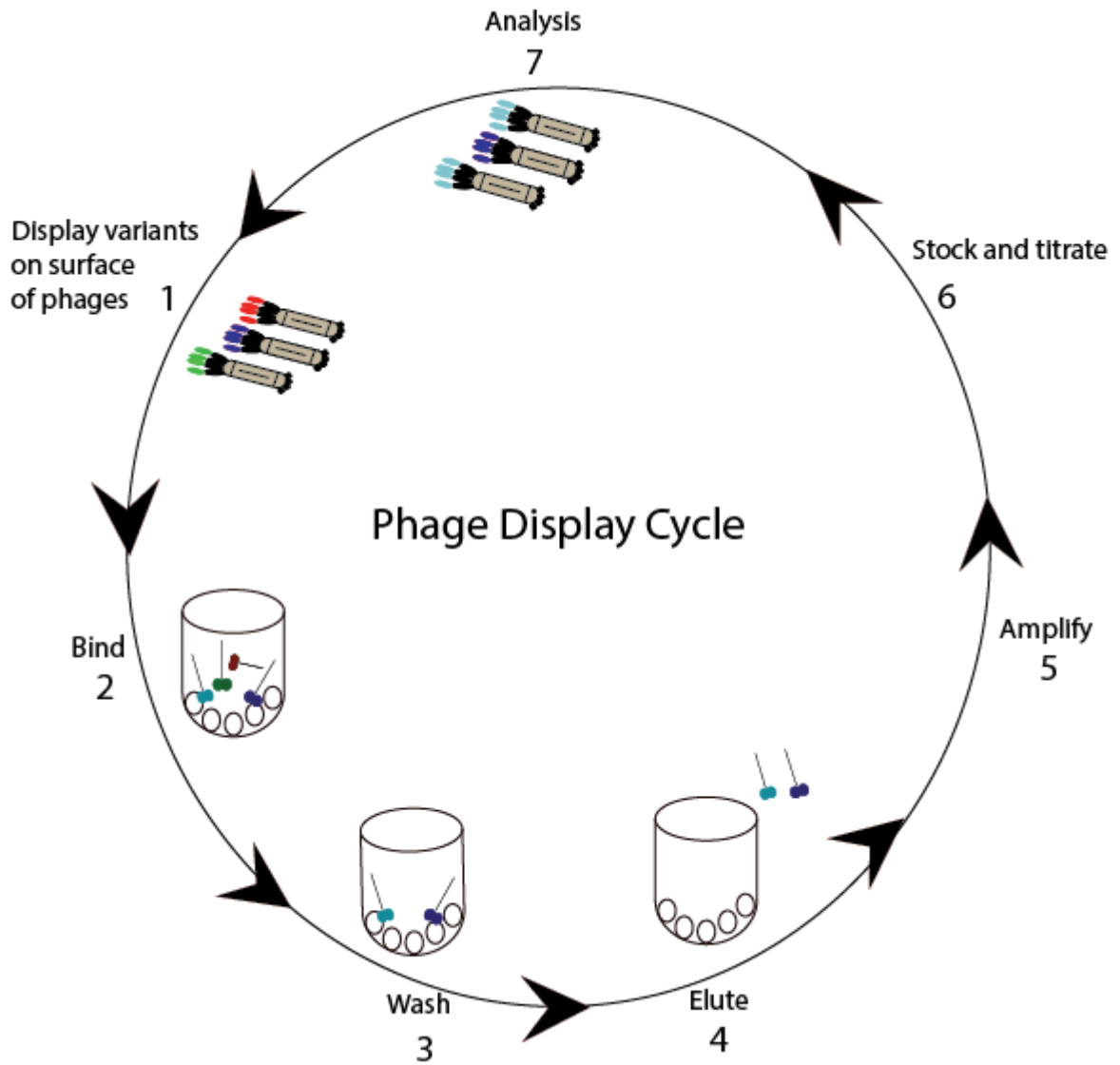
Figure 2-2. The basic phage display cycle. The basic phage display cycle consists of 6 iterative steps of several rounds, with the final step (7) of analyzing the phage bound with high affinity to the target cells. See text for detailed descriptions.
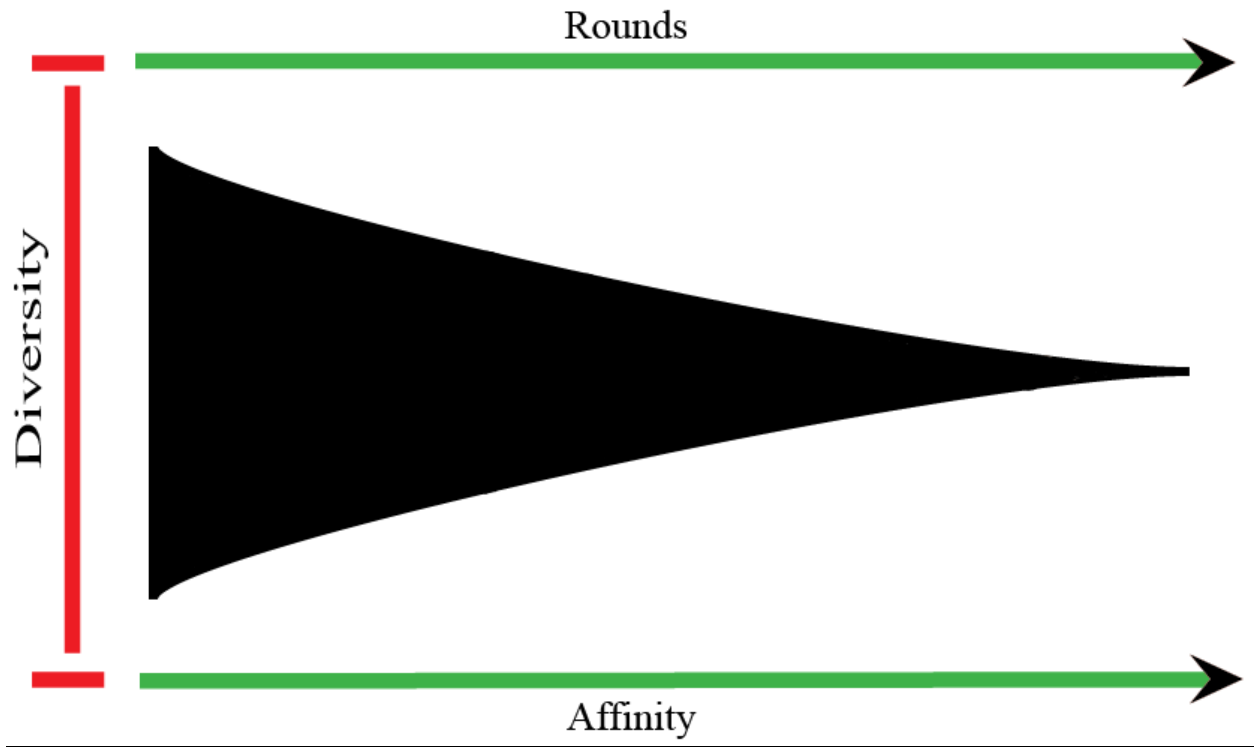
Figure 2-3. Relationship between phage diversity vs. phage affinity as a function of rounds of phage library screening. As the rounds of the phage display screening increase, the affinity of the bacteriophages/peptides to the target cells also increases, but the diversity of bacteriophages/peptides decreases.

2.2 Phage display applications

The peptides that are uncovered when using the phage display technique are, in general, specific to biologically relevant sites such as enzyme active or allosteric sites, therefore binding to these sites may interfere with their function [91]. Since phage display was first described it has influenced many scientific fields including but not limited to, drug discovery [92,93,94,95,96,97,98], drug target validation [99,100], identification of enzyme substrates and inhibitors [101,102], epitope mapping [103], selection of new antibodies and antibody surrogates as fragments on scaffold proteins[104,105], and finding new agents for delivery of gene therapy and gene therapy[106,107].

One major application for phage display is the screening against whole cells to reveal peptides that are specific to certain populations. The majority of these screenings has been performed using cancer cells with the goal of discovering novel peptides that specifically bind tumor-specific receptors and could eventually be used for the targeted delivery of therapeutics [108,109,110,111,112]. Phage display screening using whole cells comes with some caveats that must be understood. For example, the composition of the plasma membrane is very complex, containing many different protein and carbohydrate structures that could be acting as a decoy, thus concealing the cell surface molecule of interest. Consequently, only those peptides that bind receptors of relatively high cell surface density can be recovered after 3-4 rounds of purification.

A prime example of whole cell phage display screening and isolation of a peptide that is being developed for therapeutic use is described by the Arap's lab in their efforts to isolate peptides that interact with VEGFR1 and neuropilin-1 [113]. They first incubated unstimulated human umbilical vein endothelial cells (HUVEC) with the phage display

library, thus depleting non-specific binders. They then incubated the VEGF-stimulated HUVEC cells. Three rounds of selection led to the isolation of peptide, CPQPRPLC, that interacted with both VEGFR1 and NRP1 [113]. A later follow-up study revealed that only a portion of that peptide, the tripeptide RPL, was required for binding to both of the receptors [114]. Due to its small size, this peptide is being developed into a new class of VEGFR inhibitors.

In contrast to *in vitro* phage screening in cultured cells, *in vivo* phage display is conducted in which the phage libraries are injected into laboratory animals followed by collection of tissues for elution of the bound phages after a certain period of systemic circulation. Obviously, the injected phages must be able to penetrate the vascular endothelium to gain access to the tissue of interest. Theoretically, by injecting the phage library into the animal, the organs should capture many of the bacteriophages that may be of interest. A variation of the *in vivo* method is *ex vivo* phage display, in which the tissue or the tumor is excised, dissociated into single cells, and then incubated with the phage library. This latter approach eliminates the vascular endothelial barrier and also prevents excess loss of phages due to direct capturing of the phage particles by different organs.

Dr. Kolonin's lab has successfully adapted the *in vivo* phage display technique to identify peptides that specifically home in to the adipose stromal cells (ASCs), the mesenchymal progenitors in white adipose tissue [115]. After injecting the mouse with the phage display library, tissues were dissociated and then they purified out the ASCs. After four rounds of enrichment and purification, a peptide (CSWKYWFGEC) that specifically bound the ASCs was identified [115]. Using affinity chromatography, the authors found that

this peptide was binding to a previously unreported cleavage product of decorin and was mimicking resistin [115].

Developing therapeutics is one of the main applications of phage display technology. Two of the most studied therapeutic drugs that have been developed by screening phage display libraries are Hematide (also referred to as Affymax), which is the PEGylated erythropoietin receptor and Nplate (also referred to as Amgen), which is Fc-fused thrombopoietin receptor. Two other drugs in development are adalimumab, which is an anti-TNF-α antibody [116] and ecallantide, which is an inhibitor of plasma protease kallikrein [117]. These drug discoveries, along with others, suggest that the phage display library screening is a relevant technique for discovering new therapeutics.

Chapter III

Phage Display Library Screening to Identify Peptides that Home in to Undifferentiated (PSA$^{-/lo}$) and Castration-Resistant Prostate Cancer Stem Cells

3.1 Introduction

Current therapies for advanced and metastatic PCa patients aim to stop androgen synthesis and/or androgen receptor (AR) signaling. These treatments, referred to as androgen deprivation therapy (ADT), reduce the primary tumor volume and serum PSA (prostate specific antigen) levels. Unfortunately, the vast majority of these patients eventually develop castration-resistant PCa (CRPC). This observation is critical because the initial treatment reduces PCa cells that express PSA. The fact that many of the tumors return may indicate that the cell-of-origin of the recurrent and CRPC resides in the population of PCa cells that do not express PSA or express it at a very low level (i.e., PSA$^{-/lo}$ cells). Our lab has provided evidence that some PSA$^{-/lo}$ PCa cells indeed exhibit many CSC characteristics.

3.1.1 Prostate specific antigen (PSA)

PSA is largely regulated by androgens. It is a member of the tissue kallikrein family. PSA is normally produced by terminally differentiated, luminal epithelial cells and secreted into the prostatic lumen. PSA is a constituent of semen, and functions to cleave semenogelins in the seminal coagulum, which mediate gel formation of semen [118]. One of the early events in PCa development is the disruption of the basal cell layer and the basement membrane. This causes loss of integrity of the normal prostatic architecture and may lead to the leakage of PSA into the peripheral circulation [118]. For this reason, PSA is used as a biomarker to detect PCa and to determine the patient's response to treatments.

To separate and compare PCa cells that express high (PSA$^+$) versus low/no (PSA$^{-/lo}$) levels of PSA, we made use of a PSAP-GFP lentivector in which the PSA promoter (PSAP)

drives eGFP expression [119]. Using this vector, LNCaP and other PCa cells were infected at multiplicity of infection (MOI) of 25, at which essentially all cells are infected. Purified GFP$^+$ PCa cells express high levels of PSA mRNA and protein whereas GFP$^-$ PCa cells express no or low levels of PSA mRNA [62]. Therefore, the PSAP-GFP lentiviral reporter system faithfully reports endogenous PSA expression and PSA$^+$ correlates with GFP$^+$ positivity and PSA$^{-/lo}$ correlates with GFP negativity.

3.1.2 Characteristics of PSA$^{-/lo}$ cells

When assessing potential contributions of PSA$^{-/lo}$ cells to PCa, our lab first performed a semi-quantitative PSA imunohistochemical (IHC) analysis [62]. Different cohorts of patient PCa slides were collected and stained for PSA, which included untreated Gleason grade (GS7, n = 10), untreated Gleason grade 9 and 10 (GS9 and GS10, n = 10), and treatment failed and CRPC (n = 23) samples. In GS7 tumors, most areas stained positive for PSA, but scattered areas of poorly differentiated tumors cells showed no PSA expression [62]. When we assessed GS9 and GS10 tumor samples, most tumor cells were undifferentiated and PSA$^{-/lo}$ with only a few areas having PSA$^+$ cells. In treatment failed and CRPC cohorts, some samples resembled the advanced grade GS9 and GS10 tumors, but the majority of samples completely lacked PSA expression [62].

LNCaP cells that were infected with PSAP-GFP and cultured in androgen deprivation conditions, either with charcoal dextran-stripped serum (CDSS) or with an anti-androgen (bicalutamide), contained a PSA$^{-/lo}$ cell population that expanded whereas the PSA$^+$ cell population decreased [62]. We also used whole-genome transcriptome profiling of purified PSA$^+$ cells and PSA$^{-/lo}$ cells to uncover genes that were preferentially expressed in each population. The PSA$^{-/lo}$ cell population was enriched in anti-stress genes and also

overexpressed Bcl-2, an anti-apoptotic gene. Further experiments showed that the PSA$^{-/lo}$ cells were resistant to androgen deprivation, chemotherapeutic drugs, and also other stress treatments [62].

Comprehensive studies in 5 PCa xenograft models and a dozen of primary PCa derived cells demonstrate that the PSA$^{-/lo}$ PCa cells exhibit many characteristics of SCs. For example, they underexpress dozens of mitosis and cell-cycle genes, suggesting these cells may be more quiescent than the PSA^{+} cells [62]. Indeed, prospective label-retaining experiments and cell-cycle analysis reveal that PSA$^{-/lo}$ PCa cells have cell-cycle transit times several fold longer than that in corresponding PSA^{+} PCa cells [62]. In addition, PSA$^{-/lo}$ cells overexpress many stem cell and developmental markers, including ASCL1, CTED2, GATA6, IGF-1R, KLK5, LRIG1, and NKX3.1 [62]. Another SC characteristic these cells possess is their ability to self-renew. Purified single PSA^{+} and PSA$^{-/lo}$ cells were plated and their expansion was monitored for 4 weeks. The clones from the PSA^{+} cells remained 100% GFP positive, but the PSA$^{-/lo}$ cells developed into three distinct types of clones. The first type of clones consisted of all GFP^{+} cells, second type both GFP^{+} and GFP^{-} cells, and third type only GFP$^{-/lo}$ cells [62]. Another way to examine self-renewal capacity was time lapse videomicroscopy, in which single cells from each population were tracked. The results showed that GFP^{+} cells only gave rise to other GFP^{+} cells, but GFP$^{-/lo}$ cells generated both GFP^{+} and GFP^{-} PCa cells [62]. Conclusively, this data showed that PSA$^{-/lo}$ cells do have SC characteristics and the ability to undergo asymmetric cell division.

3.2 Material and Methods

Cells

LNCaP cells were obtained from ATCC and cultured in RPMI containing 7% FBS, 100 µg/ml streptomycin, and 200 U/ml penicillin (Life Technologies, Grand Island, NY).

Phage Library Screening

Competitive assay

Random peptide libraries in the bacteriophage vector fUSE5 that display inserts CX_7C (i.e, a random 7 amino acid peptide between 2 cysteine residues) and CX_8C (i.e, a random 8 amino acid peptide between 2 cysteine residues) were obtained from Dr. Mikhail Kolonin [115]. These 2 phage libraries were mixed (1:1) and incubated in 1 ml RPMI + 1% BSA with LNCaP PSA-GFP cells in suspension at 1×10^{10} phage particles per 250K cells for 1 hour at 37° C. At the end, LNCaP PSA-GFP cells were separated into GFP^+ and $GFP^{-/lo}$ cell populations by FACS using a FACSAria/sorter (BD Biosciences, San Jose, CA). Purified cells were lysed in 20 µl of H_2O, and both cell lysates were then incubated with 500 µl of competent K91 bacteria for 1 hour at RT. The bacteria were then incubated overnight on agar plates containing tetracycline (20 mg/ml) and kanamycin (100 mg/ml). Afterwards, the colonies were collected and amplified overnight in 250 ml of LB broth containing tetracycline (20 mg/ml) and kanamycin (100 mg/ml). The broth from both populations were centrifuged at 4,000 RPM for 30 min at 4°C. Next, the supernatants were filtered through 0.45 um filter. The supernatants were incubated with PEG/Nacl solution overnight at 4°C. The bacteriophages were centrifuged at 13,000 RPM for 40 minutes and re-suspended in 1 ml of PBS. After both stock bacteriophage libraries were titered using serial dilutions

followed by incubation with competent K91 bacteria for 1 hour at RT, they were incubated overnight on plates containing tetracycline and kanamycin [120]. In the next 3 rounds, both GFP$^+$ and GFP$^{-/lo}$ bacteriophage libraries were mixed (1:1) and incubated in 1 ml RPMI + 1% BSA with LNCaP PSA-GFP cells at a total concentration of 1×10^{10} per million cells for 1 hour at RT. Finally, after a total of 4 rounds of purification, 287 bacterial colonies from each population were sequenced (Lone Star Labs, Houston, TX).

Indirect subtraction assay

The indirect subtraction method is similar to the competitive assay but modified in a few key aspects. First, we used adherent LNCaP PSA-GFP cells instead of cells in suspension. Second, for the initial incubation with the CX$_7$C and CX$_8$C libraries, a total concentration of 1×10^{12} phage particles per million cells was utilized. Third, for the other 3 rounds of purification we only utilized the bacteriophage library derived from the GFP$^{-/lo}$ cells and incubated each round with a total concentration of 1×10^{10} phage particles per million cells. Finally, we decided to sequence bacterial colonies from the third round instead of the fourth round of purification.

Direct subtraction assay

The direct subtraction method is similar to the indirect subtraction assay but also modified in a few aspects. First, we incubated the LNCaP PSA-GFP cells AFTER they had been sorted into GFP$^{-/lo}$ and GFP$^+$ populations. Second, for the initial incubation with the CX$_7$C and CX$_8$C libraries a total concentration of 2×10^9 phage particles per million cells was utilized. Also, we first incubated the GFP$^+$ cells with the phage particles for 1 hour at 37˚C and then we took the supernatant and incubated the GFP$^{-/lo}$ cells for 1 hour at 37˚C.

Third, for the next 3 rounds we only utilized the bacteriophage library derived from the GFP$^{-/lo}$ cells at a concentration of 2×10^9 phage particles per million cells, and incubated them with the GFP$^+$ cell for 1 hour at 37˚C before collecting the supernatant and incubating the remaining library with the GFP$^{-/lo}$ cells. Finally, we sequenced 150 bacterial colonies from each population from the fourth round (Lone Star Labs).

In vivo phage display assay

Male Nod/Scid mice were used. Mice were orthotopically implanted with LAPC9 cells in the DP. Once the tumors became palpable, mice were injected via tail vein with the CX$_7$C and CX$_8$C libraries (1:1; the combined 1×10^{10}). The liver and lungs were collected as controls, and tumors were excised. Tumors were subjected to enzymatic digestion as described [121] dissociate tumor cells were separated into the GFP$^+$ and GFP$^{-/lo}$ cell populations by FACS. Purified cells were lysed using dounce homogenizer or H$_2$O. The subsequent steps were similar to those in the competitive assay except that we only utilized bacteriophage libraries derived from the GFP$^{-/lo}$ LAPC9 cells. In addition, we re-injected the libraries in the tail vein and let the injected libraries to circulate for 2 hours. Remaining steps were similar to those described in the competitive assays.

Cell Analysis by Immunofluorescence

Regular and biotinylated peptides (JRM0, JRM1, JRM2) were chemically synthesized and purified to at least 95% purity (Genemed Synthesis Inc., San Antonio, TX). FACS-purified GFP$^+$ and GFP$^{-/lo}$ LNCaP cells were plated on glass coverslips and incubated with the peptides at a concentration of 200 nM/100K cells in RPMI+1% BSA for 1 hour at 37˚C, and then washed twice. Cells were incubated with Alexa fluor-594 for 30 minutes at RT, and

washed twice. At the end, cells were fixed with 4% PFA for 15 minutes at RT. Cells were counterstained with DAPI and slides mounted in Prolong Gold Anti-Fade (Invitrogen, Grand Island, NY). Finally, fluorescence images of the cells were acquired with an Olympus IX71 microscope.

Cell Analysis by Confocal Microscopy

The JRM2 peptide was conjugated with Lassamine Rhodamine (JRM2-LR). FACS-purified GFP$^+$ and GFP$^{-/lo}$ cells were plated on coverslips and incubated with JRM2-LR at a concentration of 200 nM/100K cells in RPMI+1% BSA for 1 hour at 37°C and then washed twice. Cells were fixed with 4% PFA for 15 minutes at RT. After DAPI counterstain, coverslips were washed three times and mounted in Prolong Gold Anti-Fade on a microscope slide. Confocal microscopy was done on a Zeiss LSM510 META confocal microscope with 63X plan-apochromatic objective and oil immersion. Images were acquired in sequential mode.

Cell Analysis by FACS

Bulk LNCaP cells infected with the PSAP-GFP lentivector were incubated with biotinylated JRM0, JRM1 and JRM2 peptides at 200 nM/100K cells in RPMI+1% BSA for 1 hour at 37°C followed by washing twice. Subsequently, cells were incubated with Strepavidin-APC (BD Biosciences) (1:500) for 30 minutes at RT. Next, analysis was performed with BD LSR Fortessa-Cell Analyzer. Afterwards, JRM1 and JRM2 peptides were conjugated to aminocoumarin (AMC), and LNCaP PSA-GFP cells were incubated with JRM1-AMC or JRM2-AMC at 200 nM/100K cells in RPMI+1% BSA for 1 hour at

37˚C followed by washing twice. Analysis was completed using BD LSR Fortessa-Cell Analyzer.

3.3 Results

We **hypothesize** that PSA$^{-/lo}$ cells will express unique cell surface molecules and that these markers that can be identified by phage display mediated peptide binding. We utilized LNCaP cells that had been infected with PSAP-eGFP lentivector reporter, which allowed the purification of PSA$^{-/lo}$ and PSA^{+} cells [62]. We used the phage display technique to attempt to uncover peptides that could preferentially or selectively bind to the PSA$^{-/lo}$ cells. The identified peptides could theoretically be conjugated to (pro)drugs to treat CRPC.

Most advanced PCa, upon ADT treatment, show good clinical response initially but the majority of the cancers return. Thus, developing new therapeutics that target the cells responsible for this relapse is necessary. As a first step to achieve this goal, I applied phage display library screening technology to PSAP-GFP infected LNCaP cells (Fig. 3-1). We obtained two random peptide libraries CX$_7$C and CX$_8$C, from Dr. Mikhail Kolonin [115], which, when combined, could allow me to screen over 10^{11} combinatorial peptides displayed on the PIII protein of filamentous M13 bacteriophage. Herein I describe the assays we used to uncover two potential peptides that showed preferential binding to the PSA$^{-/lo}$ LNCaP cells.

3.3.1 Competitive assay: Identification of JRM1 peptide

The first assay completed was a competitive assay. After the initial incubation with the two peptide libraries (CX$_7$C and the CX$_8$C), which were mixed together at a 1:1 ratio for the first round, each of the following rounds was started by incubating the LNCaP PSA-GFP cells with a 1:1 mixture of both the GFP$^{-/lo}$ and the GFP^{+} peptide libraries that were collected from the previous round (Fig. 3-2). The main advantage of utilizing this assay is its

stringency. Since I mixed both GFP$^+$ and GFP$^{-/lo}$ phage libraries at 1:1 ratio before each round, by the fourth round if a peptide sequence unique to the GFP$^{-/lo}$ population was found, then the chance of it being of true relevance was very high.

In the initial round, we combined both the CX$_7$C and CX$_8$C libraries [115], to a total phage concentration of 1×10^{10} per 250K LNCaP PSA-GFP cells. After sorting the bottom 5% GFP$^{-/lo}$ and the top 10% GFP$^+$ cells, we obtained 500 bacterial colonies that equaled 0.009 transforming units (TU) per cell from the GFP$^{-/lo}$ population and 1,200 bacterial colonies (0.007 TU/cell) from the GFP$^+$ population. With this, we continued to the second round of purification. With these colonies, we then made each of the corresponding phage libraries and incubated LNCaP PSA-GFP cells in suspension with a 1:1 mixture of both libraries at a total phage concentration of 1×10^{10} per million cells. This round yielded 12,000 colonies (0.21 TU/cell) from the GFP$^{-/lo}$ population and 140,000 colonies (1.01 TU/cell) from the GFP$^+$ population. This result indicate that the affinity of the selected peptides increased from round one to round two. In the next round, the GFP$^{-/lo}$ cells yielded 21,800 colonies (0.39 TU/cell) and the GFP$^+$ cells yielded 120,000 colonies (0.7 TU/cell). In the fourth round, the GFP$^{-/lo}$ population yielded only 58,800 colonies, but the TU per cell equaled 1.96. The GFP$^+$ population yielded 440,000 colonies (6.29 TU/cell) (Fig. 3-2, 3-3). After four rounds of purification, we collected 287 bacterial colonies from each population, amplified the inserts by PCR, and had them sequenced.
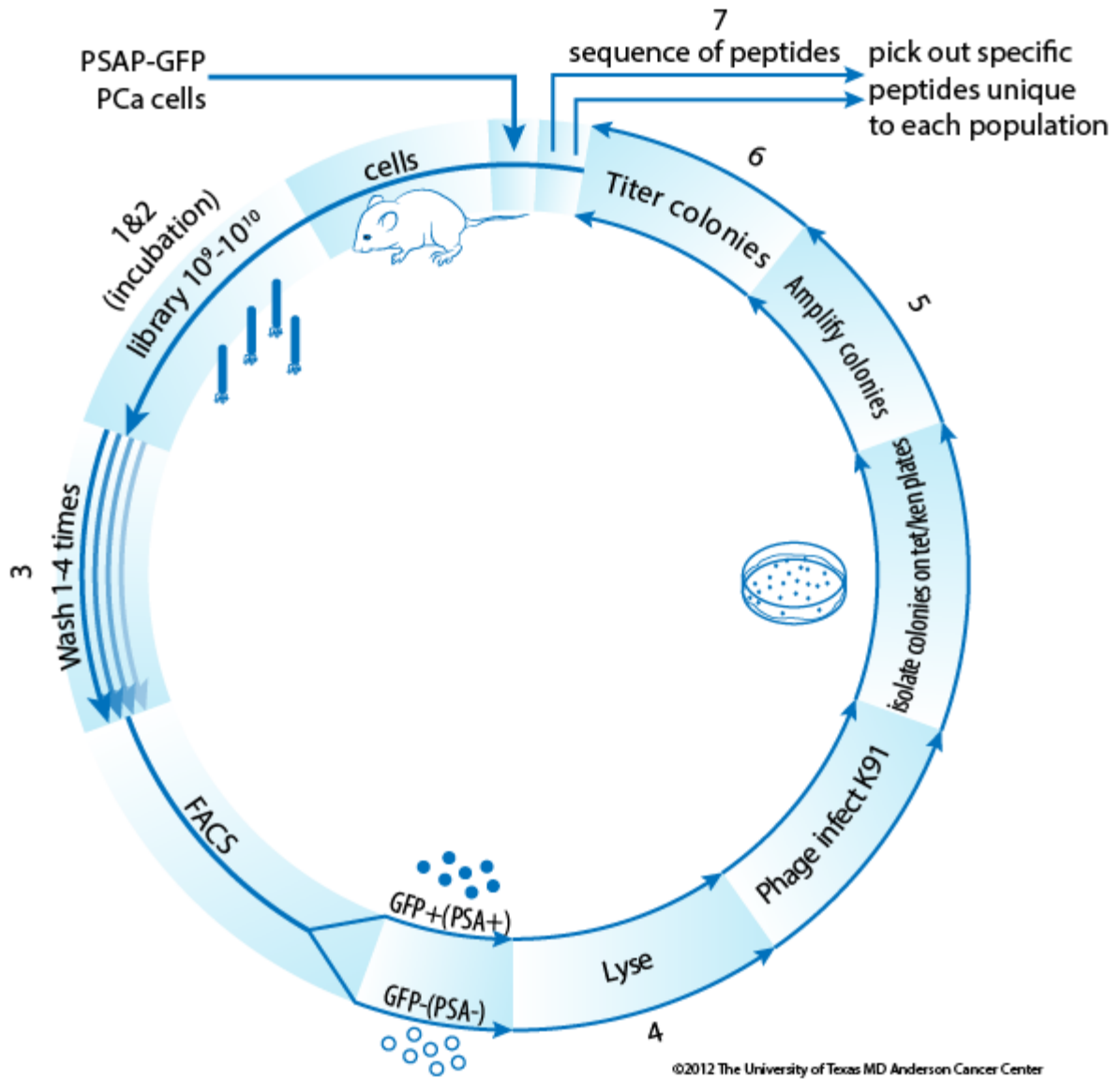
Figure 3-1. Experimental scheme for my phage display screening. Diagram including all relevant steps in my experimental scheme, from the initial incubation of LNCaP PSAP-GFP cells with phage display libraries (CX$_7$C and CX$_8$C) (steps 1 and 2), to amplifying colonies in LB broth and titering the colonies by preforming serial dilutions on K/T plates (steps 5 and 6). Finally, we selected bacterial colonies from each population for sequencing (step 7).

A

B
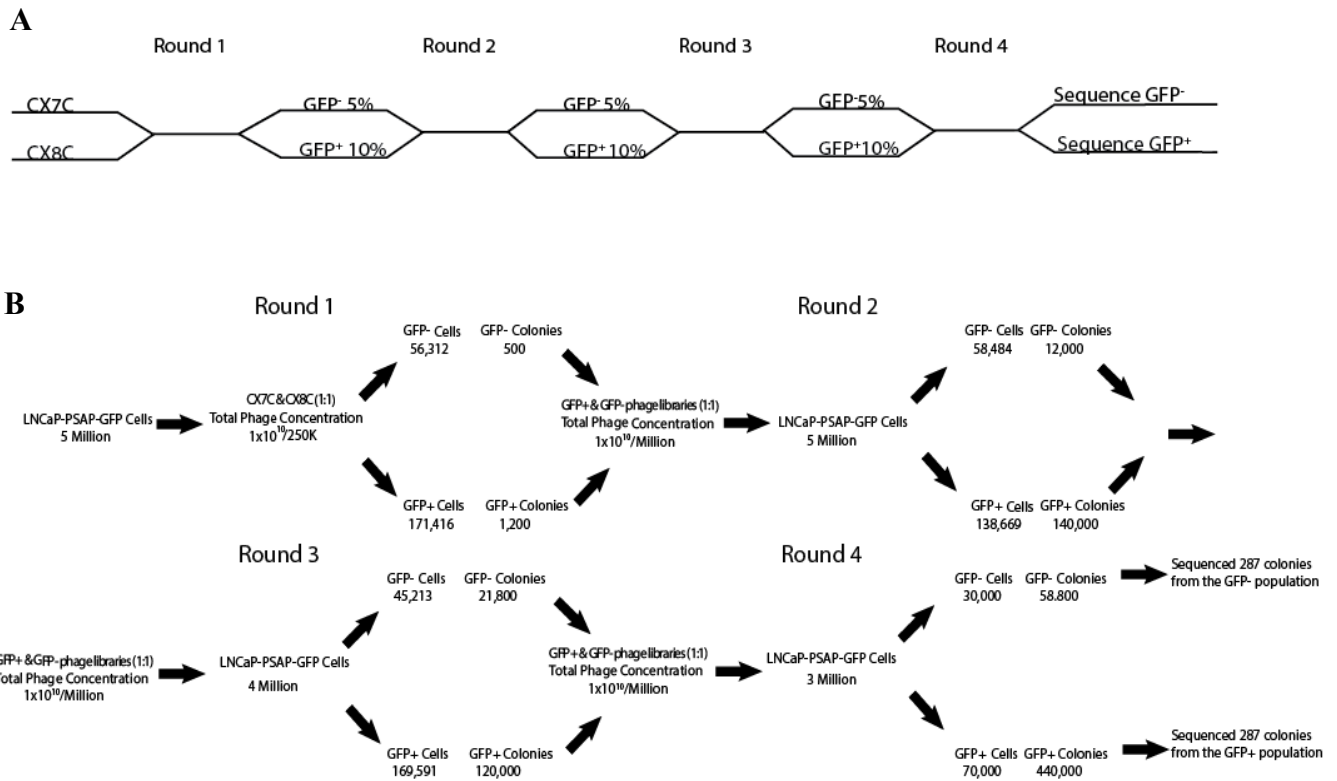
Figure 3-2. Competitive assays used to find unique peptides that bind the PSA$^{-/lo}$ LNCaP cells.

(**A**). Experimental design of competitive assay.

(**B**). Summary of the results from competitive assay, including phage concentrations, cells obtained from FACS, and colonies collected after each round of purification.
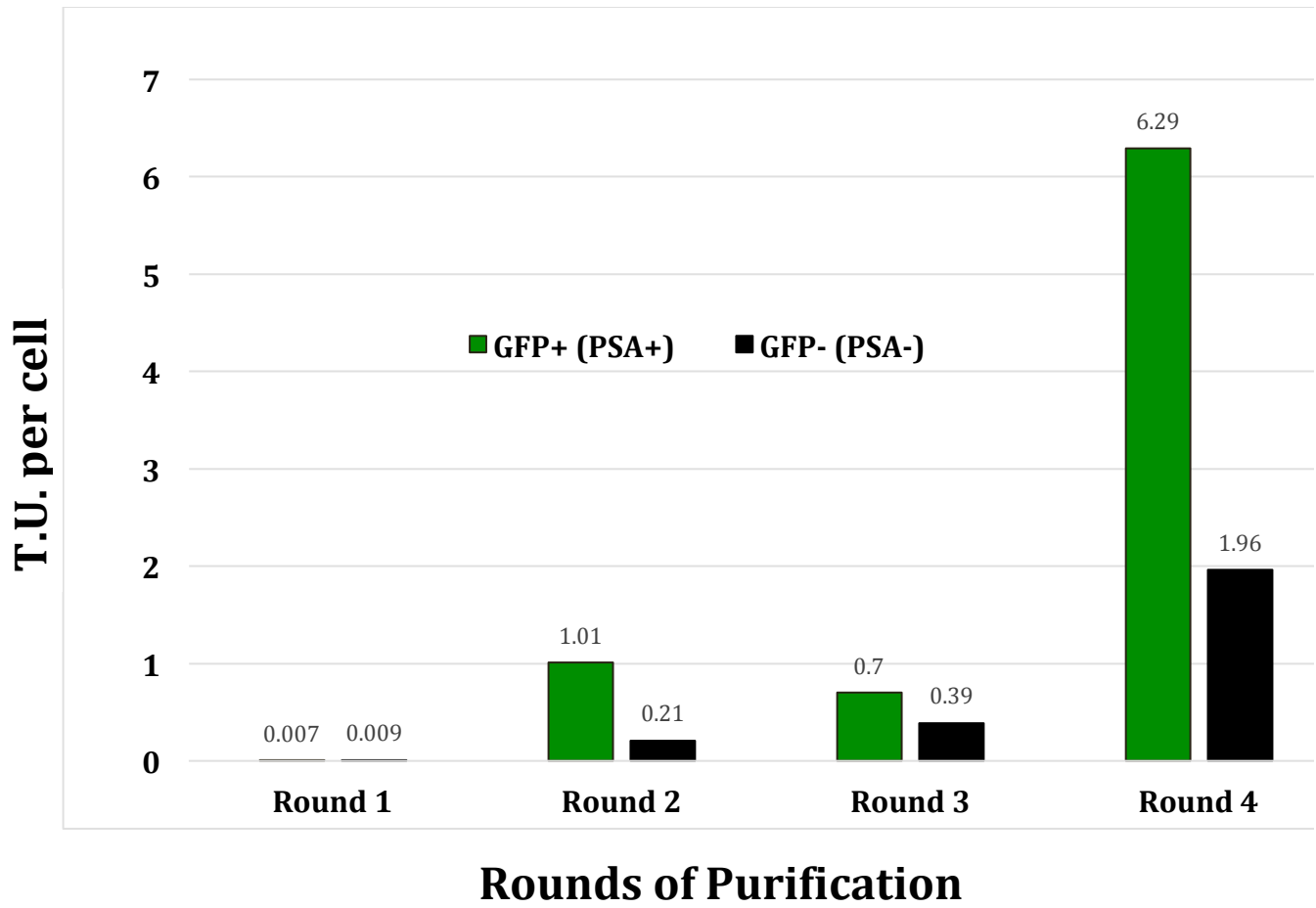
Figure 3-3. Transforming units per cell obtained at each round of purification in the competitive assay. See text for more descriptions

After all of the colonies were sequenced, we aligned the sequences using flanker regions, which are located on either side of the insert. Depending on which library the peptide was derived from, the insert can be composed of either 21 or 24 nucleotides (Fig. 3-4, A). From the 576 colonies collected, we obtained 564 (~98%) readable sequences. The majority (~78%) of those sequences obtained were comprised of the following four predominant sequences: VEYDSWML, VEGDYLL, VWTEEGPL, and TEYDTMML, which were shared between the GFP$^+$ and the GFP$^{-/lo}$ LNCaP cell populations (Fig. 3-4, B). Of the remaining sequences, only 15 were from the GFP$^{-/lo}$ population alone. One peptide, TEWDYLTV, had nine colonies and were unique to the GFP$^{-/lo}$ population, so we decided to further investigate if this peptide was binding specifically to the GFP$^{-/lo}$ cells. This peptide was referred to as JRM1 (Fig. 3-4, C). A BLAST (Basic Local Alignment Search Tool) reveals that the JRM1 peptide share sequence identity or similarity to several human proteins (Fig. 3-4, D), the biological significance of which remains to be determined.

A

X₇ or X₈

1. GFP+	GGGGCT TGT GTGGAGTATGATTCGTGGATGCTT TGT GGGG
2. GFP-	GGGGCT TGT GTGGAGTATGATTCGTGGATGCTT TGT GGGG
3. GFP+	GGGGCT TGT GTGGAGGGTGATTATGTTTTGCTG TGT GGGG
4. GFP-	GGGGCT TGT GTGTGGACGGAGGAGGGGCCTCTT TGT GGGG

cysteine   21 or 24 nucleotides long   cysteine
                  depending from which
                  library it came from

flanker   flanker

B

Competitive Assay Results

Total sequenced=	576
Unreadable sequences=	10
Negative control=	2
Readable sequences=	564
Predominant sequences=	439
Less dominant/GFP+=	110
GFP- only sequences=	15

Predominant sequences

Sequences	GFP-	GFP+
VEYDSWML	110	118
VEGDYVLL	52	54
VWTEEGPL	22	31
TEYDTMML	20	32
		439 (77.8%)

C

GFP- Only Sequences

Sequences	Clones
TEWDYLTV (JRM1)	9
SEYDNMML	1
GEYDYRMV	1
WEGDYTMV	1
VEGDYGML	1
VEFDALMV	1
TEGDYIMV	1
TEGDNIKW	1
VEGDYVML	1
LGYDSWVL	1
YEWDIILW	1
VEYDStopRML	1
MEYDTRML	1
WEGDYTMV	1
TEEDNMMW	1

D

BLAST results

Description	Query cover	Max score	Total score	E value	Identity
PREDICTED: retinoid-inducible serine carboxypeptidase isoform X1	100%	21.8	21.8	13	54%
retinoid-inducible serine carboxypeptidase precursor	100%	21.8	21.8	13	54%
probable ubiquitin carboxyl-terminal hydrolase FAF-X isoform 4	75%	23.1	23.1	5.3	83%
probable ubiquitin carboxyl-terminal hydrolase FAF-Y	75%	23.1	23.1	5.3	83%
PREDICTED: probable ubiquitin carboxyl-terminal hydrolase FAF-X isoform X2	75%	23.1	23.1	5.3	83%
probable ubiquitin carboxyl-terminal hydrolase FAF-X isoform 3	75%	23.1	23.1	5.3	83%
PREDICTED: probable ubiquitin carboxyl-terminal hydrolase FAF-X isoform X1	75%	23.1	23.1	5.3	83%
PREDICTED: tumor necrosis factor receptor superfamily member 3 isoform X3	75%	20.6	20.6	32	67%
PREDICTED: tumor necrosis factor receptor superfamily member 3 isoform X2	75%	20.6	20.6	32	67%
tumor necrosis factor receptor superfamily member 3 isoform 2	75%	20.6	20.6	32	67%

Figure 3-4. Competitive assay results

(**A**). Example of sequences. Number 1 and 2 are examples of sequences shared between both the GFP⁺ and the GFP⁻/lo populations. Number 3 is an example of a sequence unique to the GFP⁺ cells whereas number 4 a sequence unique to the GFP⁻/lo population. The insert is 21 or 24 nucleotides long depending on which library it was derived from. A cystine and a flanker region on either side surround the insert.

(**B**). List of all of the sequences collected and which group they belong and a list of the four most predominant sequences.

(**C**). List of GFP⁻/lo only peptide sequences.

(**D**). BLAST results for TEWDYLTV (JRM1) sorted by query coverage.

3.3.2 Characterizations of the JRM1 peptide

We first wanted to determine if JRM1 was truly specific to the GFP$^{-/lo}$ LNCaP cells. To this end, I first purified out the bacteriophage from one of the nine JRM1 bacterial colonies. Then, I incubated the bacteriophage with LNCaP PSA-GFP cells in suspension, and sorted the top 10% GFP^{+} and the bottom 5% GFP$^{-/lo}$ cells. This was repeated several times with cells in suspension. However, the bacteriophage displaying JRM1 did not show an apparent preference to either cell population (data not shown).

Testing of JRM1 using synthetic biotinylated JRM1 peptide

To further characterize JRM1, we had this peptide synthesized and biotinylated (Genemed), which allowed us to directly quantify its binding attributes by two different methods, IF and FACS analysis. we first sorted LNCaP PSA-GFP cells into the top 10% GFP^{+} and the bottom 5% GFP$^{-/lo}$ cells. We then plated each population on coverslips and incubated with 200 nM JRM1-biotin followed by Alexafluor 594 (Fig. 3-5). When quantifying this data I counted cells that stained positive for Alexaflour 594 (which corresponds to JRM1 binding) compared to live cells, comparing six experiments the results were inconsistent and showed no statistically significant trend toward JRM1 binding to either the GFP^{+} or GFP$^{-/lo}$ LNCaP cells (Fig. 3-5, C). This inconsistency could be caused by different variables such as different lots of JRM1-biotin or amount of time stored in solution, synthetic peptides will degrade relatively quickly once in solution. To further investigate if JRM1 had any preference for GFP$^{-/lo}$ cells, we utilized FACS analysis by incubating LNCaP PSA-GFP cells in suspension with JRM1-biotin at 200 nM per 100K cells or 50 nM per 100K cells (1 hour, 37˚C) followed by staining with streptavidin-APC (Fig. 3-6). When

LNCaP PSA-GFP cells were incubated with 200 nM per 100K cells of JRM1-biotin, JRM1 bound to 2.05% of the GFP$^+$ cells and 3.05% of the GFP$^{-/lo}$ cells, respectively. When LNCaP PSA-GFP cells were incubated with 50 nM per 100K cells of JRM1-biotin, JRM1 bound to 0.91% of the GFP$^+$ cells and 1.21% of the GFP$^{-/lo}$ cells (Fig. 3-6). In conclusion, this data suggests only a slight preference for JRM1 to bind the PSA$^{-/lo}$ relative to PSA$^+$ LNCaP cells.

A

GFP-/lo JRM1-biotin 200 nM (Exp #1)

10X   40X

DAPI

Alexa fluor 594

GFP+ JRM1-biotin 200 nM (Exp #1)

10X   40X

DAPI

Alexa fluor 594

B

GFP-/lo JRM1-biotin 200 nM (Exp #5)

10X   40X

GFP+ JRM1-biotin 200 nM (Exp #5)

10X   40X

C
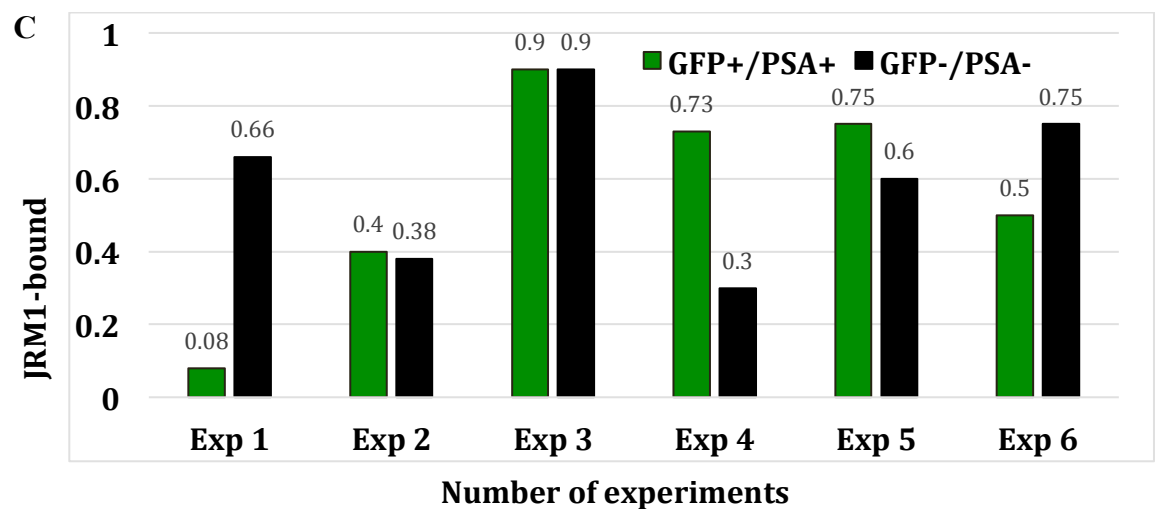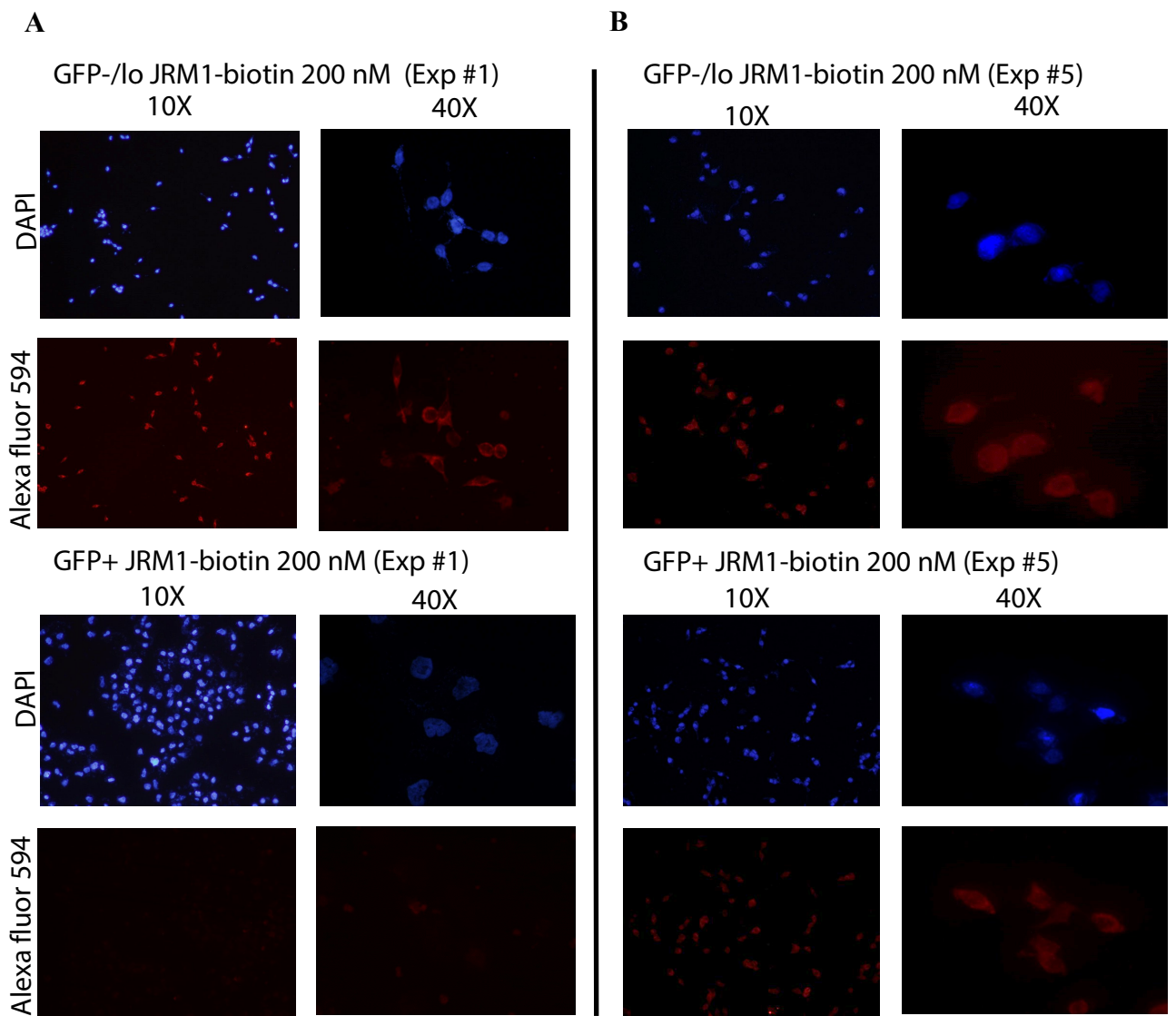
Figure 3-5. See overleaf for legend to this figure

Figure 3-5. **IF analysis of JRM1 binding to GFP$^+$ and GFP$^{-/lo}$ LNCaP cells.**

(**A**) GFP-/lo and GFP+ PSA-GFP LNCaP cells incubated with JRM1-biotin 200 nM (Exp #1) (10X) and (40X).

(**B**) GFP-/lo and GFP+ PSA-GFP LNCaP cells incubated with JRM1-biotin 200 nM (Exp #5) (10X) and (40X).

(**C**) GFP-/lo vs GFP+ PSA-GFP LNCaP cells incubated with JRM1-biotin 200 nM (bar graph of all experiments)

A

B

C
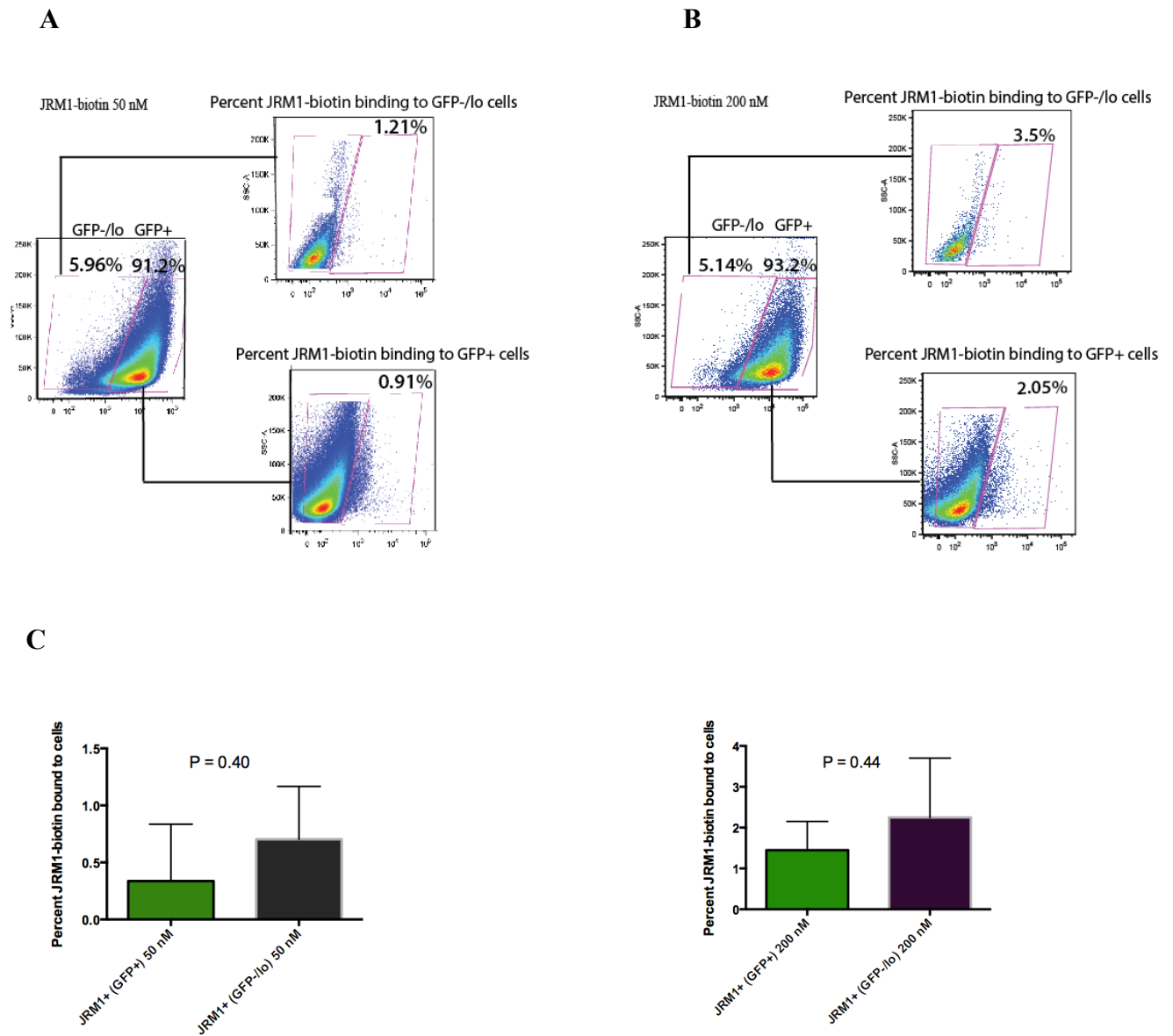
Figure 3-6. LNCaP PSA-GFP cells incubated with JRM1-biotin.

(**A**). LNCaP PSA-GFP cells incubated with 50 nM of JRM1-biotin showing only slight preferential binding to the GFP$^{-/lo}$ cells.

(**B**). LNCaP PSA-GFP cells incubated with 200 nM of JRM1-biotin showing only slight preferential binding to the GFP$^{-/lo}$ cells.

(**C**). Bar graphs showing the average binding of JRM1-biotin to the GFP$^{-/lo}$ cells versus the GFP$^+$ LNCaP cells (50 nM and 200 nM).

Testing of JRM1 using synthetic JRM1-Aminocoumarin

To further investigate the binding properties of JRM1, we had synthetic JRM1 directly conjugated to aminocoumarin (AMC). Using JRM1-AMC is a more direct method to evaluate the binding properties of JRM1. We incubated LNCaP PSA-GFP cells in suspension with 200 nM per 100K LNCaP PSA-GFP cells for one hour at 37˚C, washed twice, and then used the flow cytometry to sort out the bottom ~5% of GFP$^{-/lo}$ versus the GFP^{+} population. In the GFP^{+} population, JRM1-AMC bounds to ~0.085% of cells, and in the GFP$^{-/lo}$ population, JRM1-AMC bound to ~0.29% of the cells (Fig. 3-7). This data correlates with the data using JRM1-biotinylated peptide and suggests that the JRM1 peptide does have slight preferential binding to the PSA$^{-/lo}$ cell population relative to the PSA^{+} LNCaP cells.
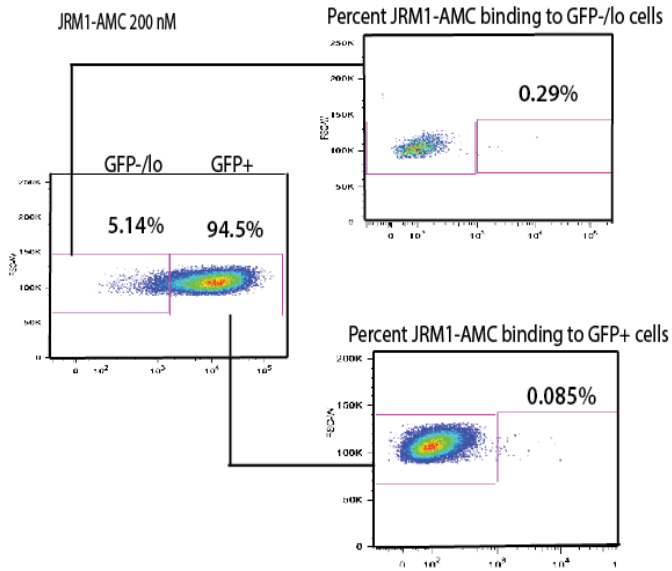
A

Figure 3-7. LNCaP PSA-GFP cells incubated with JRM1-Aminocoumarin (AMC).

(**A**). LNCaP PSA-GFP cells incubated with 200 nM of JRM1-AMC showing slight preferential binding to the GFP$^{-/lo}$ cells.

3.3.3 Indirect subtraction assay: Identification of JRM2 peptide

Given the low preferential binding of JRM1 to the PSA$^{-/lo}$ LNCaP cells, we decided to re-screen these cells using adherent cells instead of cells in suspension. Also, after the initial round of incubation with the bacteriophage libraries, we only propagated the GFP$^{-/lo}$ cell derived phages in the subsequent three rounds (Fig. 3-8). LNCaP cells are normally adherent and may display different cell surface markers when attached versus when in suspension, hence the change in my experimental approach. We only used the bacteriophages collected from the GFP$^{-/lo}$ cells in sequential screening, thereby increasing the chances of a peptide unique to the GFP$^{-/lo}$ cells being amplified each additional round. Certainly we realize that even with this screening scheme, it does not eliminate peptides that can bind both GFP$^{-/lo}$ and GFP^{+} cells.

In the initial round, we mixed both libraries CX$_7$C and the CX$_8$C, to a total phage concentration of 1×10^{12} per million LNCaP PSA-GFP cells. The higher phage concentration in the initial round was employed to obtain enough colonies to advance to the next round. It is important to note that FACS may act as stringent wash so that incubating the cells with the libraries before FACS may lead to many of the bacteriophages with lower binding affinity to be washed away during sorting. After sorting the bottom 5% GFP$^{-/lo}$ and top 10% GFP^{+} LNCaP cells, the initial round yielded 704 bacterial colonies (0.022 TU/cell) in the GFP$^{-/lo}$ population and 960 bacterial colonies (0.015 TU/cell) in the GFP^{+} population (Fig. 3-9). The 704 colonies collected from the GFP$^{-/lo}$ cells were then prepared into a secondary bacteriophage library, which was incubated with LNCaP PSA-GFP adherent cells at a concentration of 1×10^{10}/million cells. This round yielded 2,400 colonies from the GFP$^{-/lo}$ population (0.16 TU/cell) and 4,000 colonies from GFP^{+} population (0.11 TU/cell). For the

third round, we again prepared the phage library collected from the GFP$^{-/lo}$ cells and incubated it with adherent LNCaP PSA-GFP cells at a concentration of 1×10^{10} per million cells. This round yielded ~560,000 colonies (4.49 TU/cell) from the GFP$^{-/lo}$ cells and ~440,000 colonies (3.1 TU/cell) from the GFP^{+} cells. Finally in the fourth round, with the colonies collected in the third round from the GFP$^{-/lo}$ cells, we prepared its corresponding phage library and incubated it with adherent LNCaP PSA-GFP cells at a concentration of 1×10^{10} per million cells. This round yielded ~489,600 colonies (6.12 TU/cell) from the GFP$^{-/lo}$ cells and ~866,400 colonies (6.04 TU/cell) from the GFP^{+} cells (Fig. 3-8, 3-9). When comparing GFP$^{-/lo}$ to GFP^{+} TU per cell, the third round showed a higher preference toward the GFP$^{-/lo}$ population when compared to the fourth round (Fig. 3-9). Consequently we collected 287 bacterial colonies from each population of the third round, amplified the inserts by PCR and subsequently sequenced the peptide-encoding inserts.

A

B
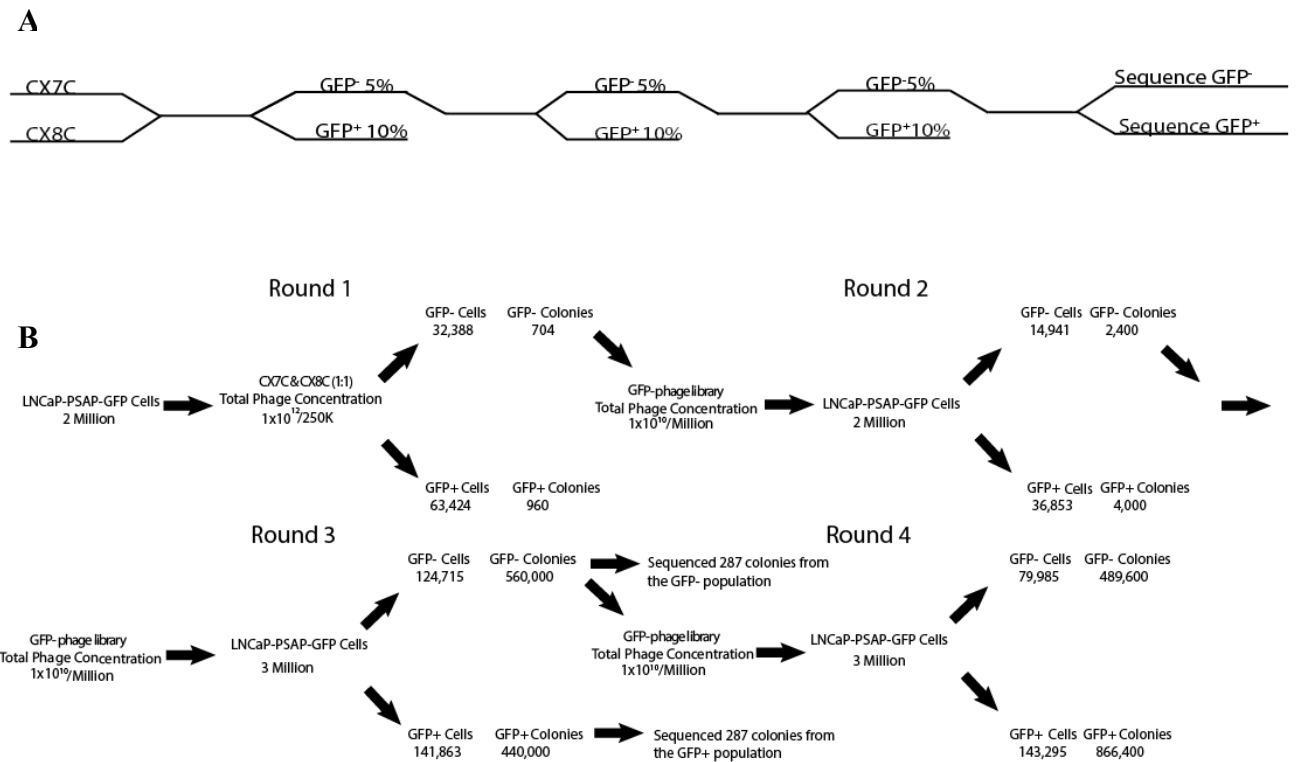
Figure 3-8. Indirect subtraction assay used to find unique peptides that attach to the PSA$^{-/lo}$ LNCaP cells.

(**A**). Experimental design of indirect subtraction assay.

(**B**). Results of the indirect subtraction assay, which include phage concentrations, cells collected after FACS, and clones collected after each round of purification.
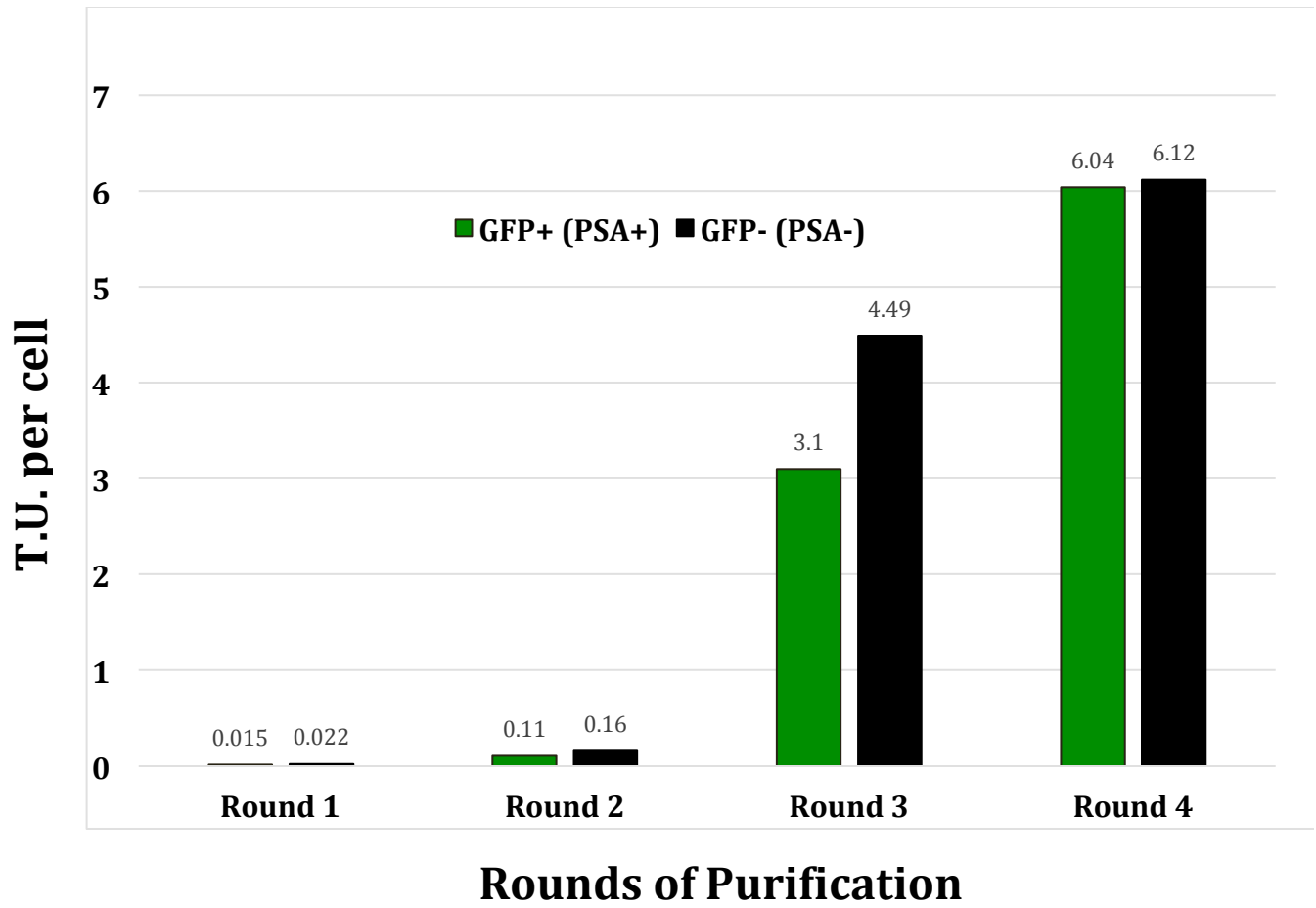
Figure 3-9. Transforming units per cell obtained at each round of purification in the indirect subtraction assay. See text for more descriptions

From the 576 colonies collected, we obtained 566 readable sequences. Of those, the majority (~98%) of the sequences were comprised of the following three predominate sequences: YEWDYLFW, VEYDAMEL, and LEFDLMLV, which all were shared between the GFP$^+$ and the GFP$^{-/lo}$ LNCaP cell populations (Fig. 3-10, A). Of the remaining sequences, 12 were unique to the GFP$^{-/lo}$ population (Fig. 3-10, B). One peptide, GFYVGQR, had two colonies that were only in the GFP$^{-/lo}$ population (Fig. 3-10, B). We subsequently chose to further investigate whether this peptide, referred to as JRM2, was binding preferentially to the PSA$^{-/lo}$ LNCaP cells.

A   Indirect Subtraction Results

Total sequenced=   576
Unreadable sequences=   8
Negative control=   2
Readable sequences=   566
Predominant sequences=   554
GFP- only sequences=   12

Predominant sequences

Sequences	GFP-	GFP+
YEWDYLFW	147	131
VEYDAMEL	73	73
LEFDLMLV	55	75
	554 (97.9%)	

B
GFP- Only Sequences

Sequences	Clones
GFYVGQR (JRM2)	2
GMAVGKWK	1
LHLLGGR	1
VEYEAME	1
YEWFPFL	1
RKREPYAS	1
WNVMGDNV	1
EAMREGFR	1
THSGTPTS	1
VVSGLWGA	1
PSRVAAWA	1

C   BLAST results (JRM2)

Description	Query cover	Max score	Total score	E value	Identity
PREDICTED: bestrophin-1 isoform X10	100%	17.6	34.4	245	55%
solute carrier organic anion transporter family member 5A1 isoform 2	100%	17.6	33.1	246	71%
solute carrier organic anion transporter family member 5A1 isoform 3	100%	17.6	33.1	246	71%
solute carrier organic anion transporter family member 5A1 isoform 1	100%	17.6	33.1	246	71%
epidermal growth factor receptor substrate 15-like 1 isoform 4	100%	17.2	17.2	335	71%
PREDICTED: epidermal growth factor receptor substrate 15-like 1 isoform X5	100%	17.2	17.2	335	71%
epidermal growth factor receptor substrate 15-like 1 isoform 3	100%	17.2	17.2	335	71%
PREDICTED: epidermal growth factor receptor substrate 15-like 1 isoform X4	100%	17.2	17.2	335	71%
PREDICTED: epidermal growth factor receptor substrate 15-like 1 isoform X3	100%	17.2	17.2	335	71%
epidermal growth factor receptor substrate 15-like 1 isoform 2	100%	17.2	17.2	335	71%
epidermal growth factor receptor substrate 15-like 1 isoform 1	100%	17.2	17.2	335	71%

Figure 3-10. Indirect subtraction assay results

(**A**). List of all of the sequences collected and which group they belong and a list of the four most predominant sequences.

(**B**). List of GFP^{-/lo} only peptide sequences.

(**C**). BLAST results for GFYVGQR (JRM2) sorted by query coverage.

3.3.4 Characterizations of the JRM2 peptide

After identifying the JRM2 peptide, we first utilized BLAST (Basic Local Alignment Search Tool) to determine whether JRM2 is identical to or overlaps with certain known peptide sequences (Fig. 3-10, C). The results revealed that JRM2 may be mimicking epidermal growth factor receptor substrate 15-like 1 isoforms 1-4. Future work will determine what protein peptides JRM2 might be mimicking and what cell surface receptors it might be binding to.

Testing of JRM2 using synthetic biotinylated JRM2 peptide

To determine if JRM2 is binding preferentially or specifically to the GFP$^{-/lo}$ LNCaP cells, we used the same experimental approach that we took with JRM1. Briefly, we had JRM2 synthesized and biotinylated and then, we sorted LNCaP PSA-GFP cells into the top 10% GFP^{+} and the bottom 5% GFP$^{-/lo}$ LNCaP cells. Each cell population was plated on coverslips and incubated with 200 nM JRM2-biotin followed by incubating with streptavidin 594 (Fig. 3-11). Strikingly, JRM2 showed preferential binding to the GFP$^{-/lo}$ LNCaP cells when compared to its binding to GFP^{+} LNCaP cells (Fig. 3-11). To further investigate the binding properties of JRM2, we utilized JRM2-biotin in conjunction with flow cytometry based quantification. To better control for this experiment, we obtained a biotinylated control peptide, called JRM0 (VEYDSWML) that showed no preference between GFP^{+} versus GFP$^{-/lo}$ cells. We incubated LNCaP PSA-GFP cells with JRM2-biotin or JRM0-biotin peptides at 200 nM per 100K cells for 1 hour at 37˚C. JRM0-biotin attached to 34.6% of GFP^{+} and 37.2% of the GFP$^{-/lo}$ LNCaP cells, indicating that, as expected, JRM0 shows similar binding towards GFP^{+} and GFP$^{-/lo}$ cell populations (Fig. 3-12, A). In contrast, JRM2 showed binding to 5.2% of GFP^{+} cells and 23.6% of the GFP$^{-/lo}$ cells, respectively (Fig. 3-

12, B). This data provides the first piece of evidence that JRM2 preferentially binds to PSA$^-$/lo LNCaP cells and warrants further investigation.

GFP- JRM2-biotin 200 nM

GFP+ JRM2-biotin 200 nM
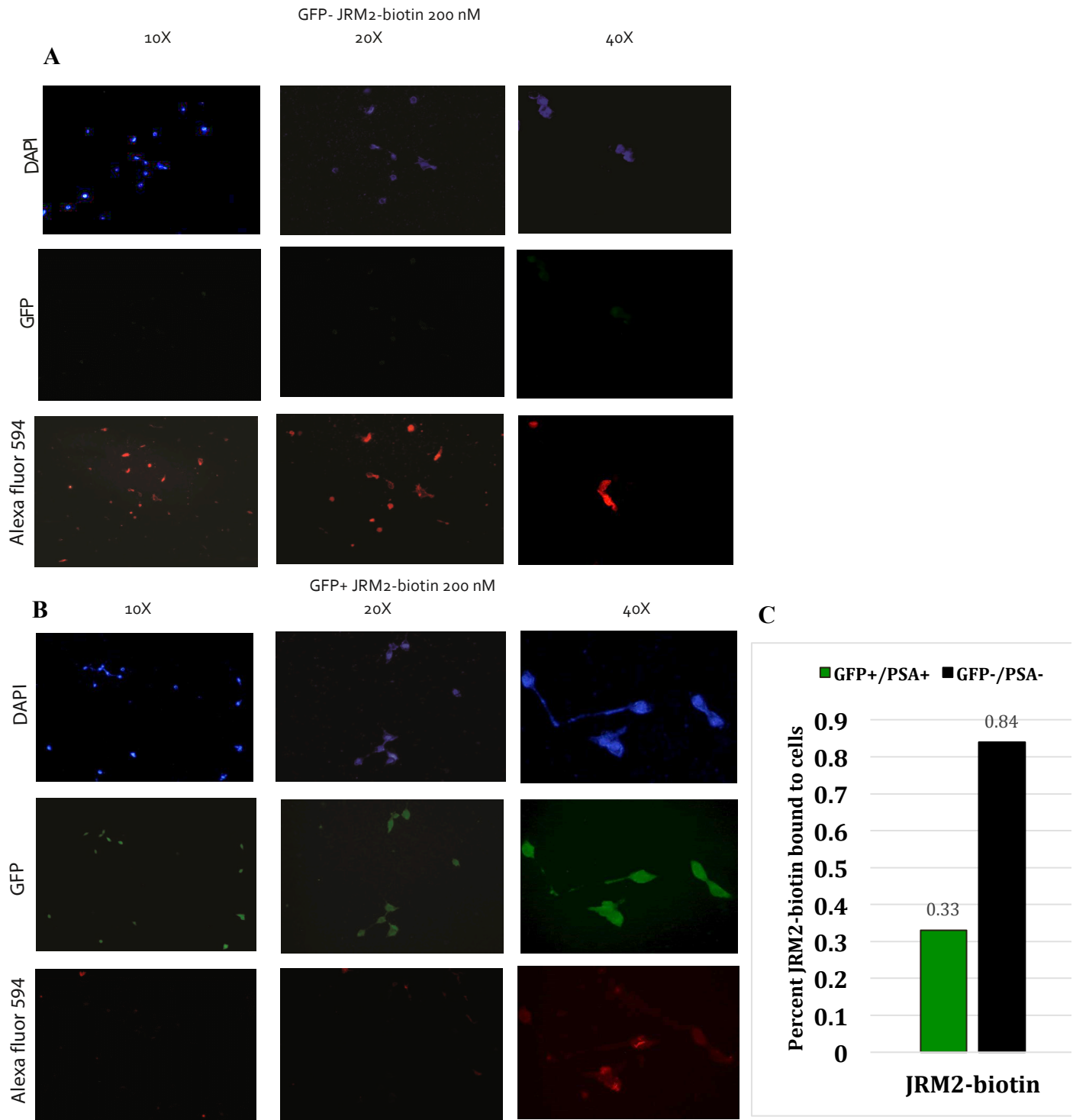
Figure 3-11. See overleaf for legend to this figure

Figure 3-11. Characterization of JRM2 binding to PSA$^+$ and PSA$^{-/lo}$ LNCaP cells by immunofluorescence.

(**A**) GFP$^{-/lo}$ PSA-GFP LNCaP cells incubated with JRM2-biotin 200 nM (10X),(40X).

(**B**) GFP$^+$ PSA-GFP LNCaP cells incubated with JRM2-biotin 200 nM (10X),(40X).

(**C**) Bar graph showing preferential binding of JRM2-biotin to the GFP$^{-/lo}$ cells versus the GFP$^+$ LNCaP cells.

Figure 3-12. LNCaP PSA-GFP cells incubated with JRM0-biotin and JRM2-biotin.

(**A**). LNCaP PSA-GFP cells incubated with 200 nM of JRM0-biotin showing no preferential binding for either GFP$^{-/lo}$ cells or GFP^{+} cells.

(**B**). LNCaP PSA-GFP cells incubated with 200 nM of JRM2-biotin showing preferential binding to the GFP$^{-/lo}$ cells.

Testing of JRM2 using synthesized JRM2-Aminocoumarin

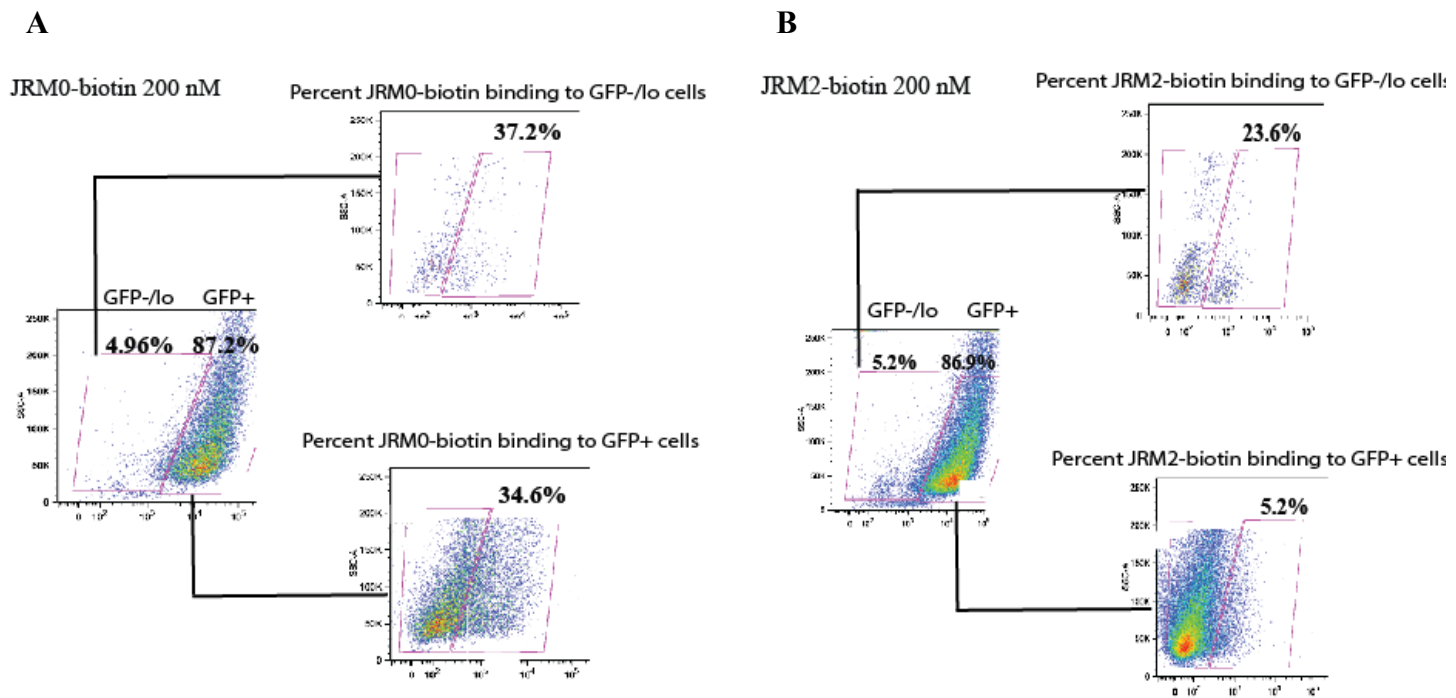To further investigate the binding properties of JRM2, we applied the same experimental strategy that we utilized with JRM1. First, JRM2 was synthesized and directly conjugated to AMC (Genemed). Subsequently, we incubated LNCaP PSA-GFP cells in suspension with the JRM2-AMC peptide (200 nM per 100K) cells and analyzed the peptide binding via FACS. We set the FACS gates utilizing LNCaP PSA-GFP cells and uninfected LNCaP cells not incubated with JRM2-AMC. JRM2-AMC bound to ~4.13% of the PSA$^+$ and ~69.6% PSA$^{-/lo}$ LNCaP cells, respectively (Fig. 3-13). These results further indicate that JRM2 peptide shows preferential binding to the GFP$^{-/lo}$ cell population.

Testing of JRM2 using synthetic JRM2-Lassamine Rhodamine

Next, JRM2 was directly conjugated to Lassamine Rhodamine (LR) (Genemed). In this experiment we utilized confocal microscopy to assess the binding properties of JRM2. We again sorted LNCaP PSA-GFP cells into the top 10% GFP$^+$ and the bottom 5% GFP$^{-/lo}$ LNCaP cells. Each cell population was plated on coverslips, and GFP$^+$, GFP$^{-/lo}$, and unsorted bulk LNCaP PSA-GFP cells were incubated with 200 nM JRM2-LR for 1 hour at 37˚C (Fig. 3-14). Strikingly, JRM2-LR bound to the majority of the GFP$^{-/lo}$ LNCaP cells when compared to the GFP$^+$ LNCaP cells (Fig. 3-14 B and C). Even when unsorted bulk LNCaP PSA-GFP cells were incubated with JRM2-LR it showed preferential binding to the GFP$^{-/lo}$ cells. This data indicates that JRM2 has strong preferential binding to GFP$^{-/lo}$ cell population (Fig. 3-14). This result, together with the data using JRM2-biotin and JRM2-AMC, confirms that the JRM2 peptide preferentially binds to the GFP$^{-/lo}$ (PSA$^{-/lo}$) LNCaP cells.
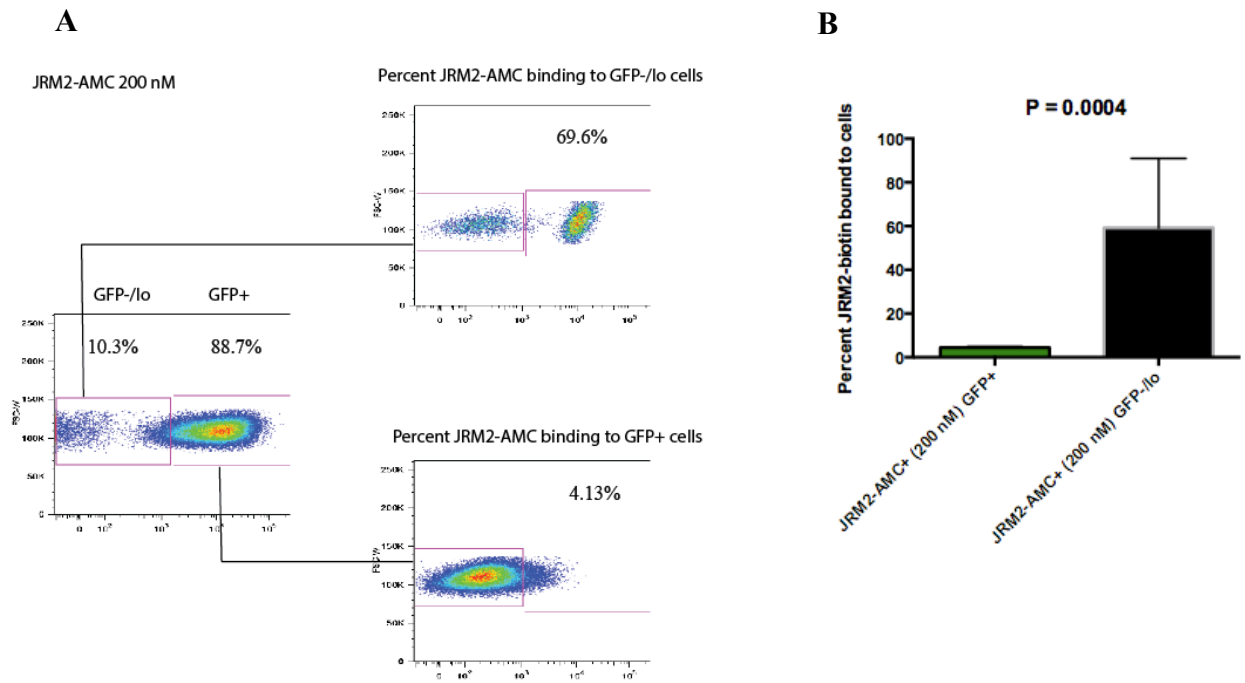
Figure 3-13. LNCaP PSA-GFP cells incubated with JRM2-Aminocoumarin (AMC).

(**A**). LNCaP PSA-GFP cells incubated with 200 nM of JRM2-AMC showing strong preferential binding to the GFP$^{-/lo}$ cells.

(**B**). Bar graph showing the average binding of JRM2-AMC to the GFP$^{-/lo}$ cells versus the GFP^{+} LNCaP cells.

Figure 3-14. Analysis of JRM2-lassamine rhodamine (LR) utilizing confocal microscopy.

(**A**). LNCaP cells utilized as negative control.

(**B**). Sorted GFP+ LNCaP PSA-GFP cells incubated with 200 nM of JRM2-LR.

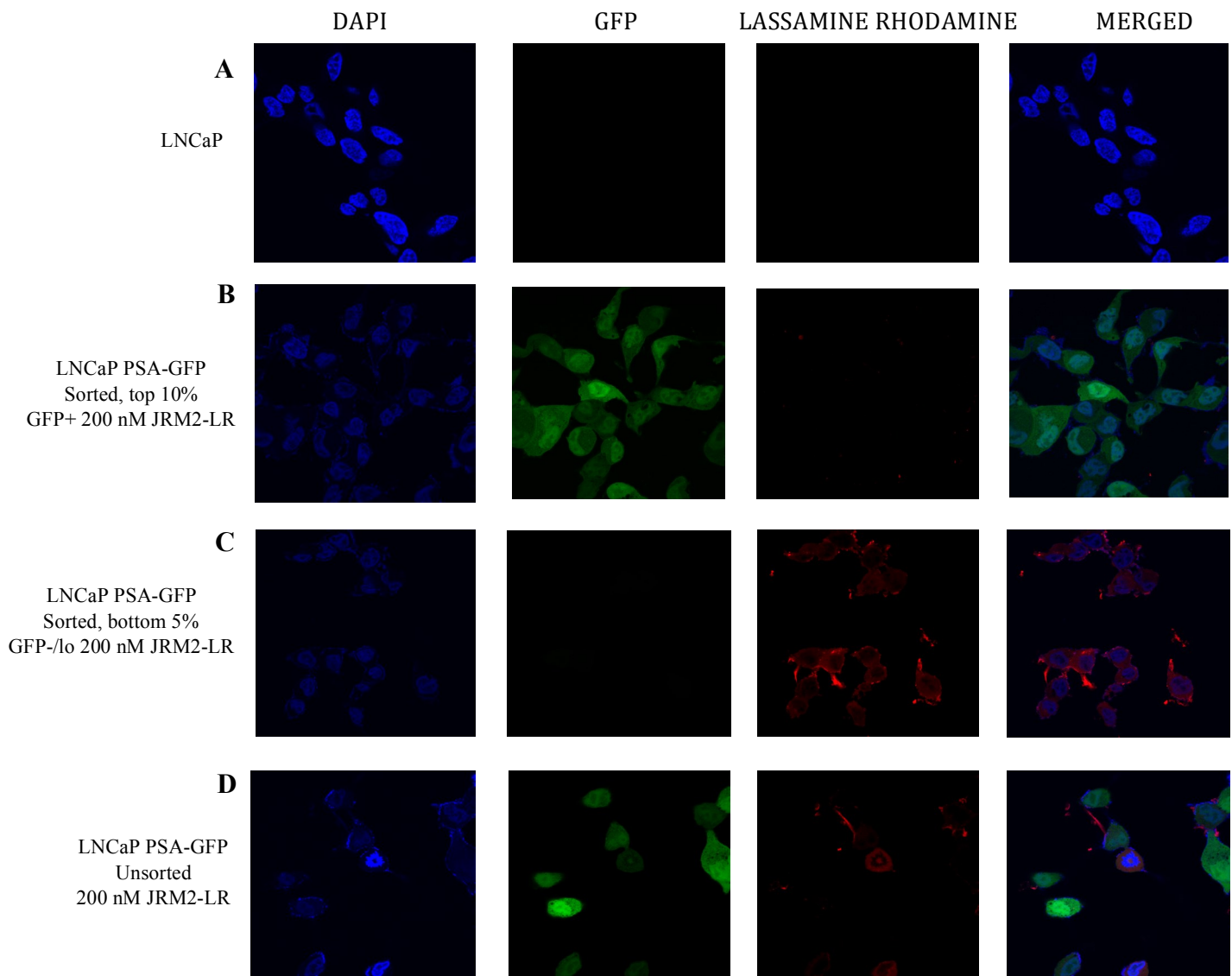(**C**). Sorted GFP- LNCaP PSA-GFP cells incubated with 200 nM of JRM2-LR.

(**D**). Unsorted LNCaP PSA-GFP cells incubated with 200 nM of JRM2-LR.

3.3.5 Direct subtraction assay

In all preceding screening experiments, infected LNCaP cells were incubated, in suspension or adherence, with the mixed phage libraries followed by flow sorting of GFP$^+$ and GFP$^{-/lo}$ cells. Since flow sorting is a very harsh process, some bacteriophages or peptides of interest might become detached during sorting. To circumvent this potential problem we employed the direct subtraction method by incubating the LNCaP PSA-GFP cells after FACS, instead of before FACS. We also let the GFP$^+$ cells act as a sink, by incubating either the initial libraries (i.e, CX$_7$C and CX$_8$C libraries) or the bacteriophage libraries derived from the GFP$^{-/lo}$ LNCaP cells, with the GFP$^+$ cells first. By doing so, the bacteriophages that bind to the GFP$^+$ cells will be depleted. The supernatant with the GFP$^+$-specific phages depleted is then incubated with the GFP$^{-/lo}$ LNCaP cells, thus increasing the likelihood of isolating bacteriophages unique to the PSA$^{-/lo}$ cell population (Fig. 3-15).

For the direct subtraction assay, in the initial round we mixed both the CX$_7$C and CX$_8$C libraries to a total concentration of 2×10^9 per million LNCaP PSA-GFP cells for 1 hour at 37˚. After sorting the bottom 5% GFP$^{-/lo}$ and the top 10% GFP$^+$ cells, the initial round yielded 26,000 bacterial colonies (0.32 TU/cell) from the GFP$^{-/lo}$ population and 23,750 bacterial colonies (0.13 TU/cell) from the GFP$^+$ population. The TU/cell is more than 10 fold higher using the direct subtraction method compared to the other two methods, suggesting that this method is probably working better. For the second round of purification, the 26,000 bacterial colonies were collected from the GFP$^{-/lo}$ cells and prepared into the secondary bacteriophage library. We again sorted LNCaP PSA-GFP into the bottom 5% GFP$^{-/lo}$ cells and the top 10% GFP$^+$ cells and then incubated the GFP$^+$ cells with this bacteriophage library after this incubation. The supernatant was collected to incubate with

the GFP$^{-/lo}$ cells. This round yielded 12,500 bacterial colonies (0.12 TU/cell) from the GFP$^{-/lo}$ cells and 25,000 bacterial colonies (0.13 TU/cell) from the GFP$^+$ cells. For the third round, we repeated the same process and obtained 17,900 bacterial colonies (0.19 TU/cell) from the GFP$^{-/lo}$ population and 18,200 bacterial colonies (0.11 TU/cell). In the fourth round, the GFP$^{-/lo}$ cells yielded ~1,400,000 bacterial colonies (12.88 TU/cell) and the GFP$^+$ cells yielded ~1,200,000 bacterial colonies (6.48 TU/cell) (Fig. 3-15 and 3-16).

We collected 150 bacterial colonies from each population of the fourth round, amplified the inserts by PCR and subsequently sequenced the peptide-encoding inserts. Strikingly, the direct subtraction assay yielded only 3 peptides that were repeated more than twice accounting for ~20% of the readable sequences (Fig. 3-10, A and 3-17, A), compared to the indirect subtraction assay in which the predominant 3 sequences accounted for ~98% of the total sequences. Also the direct subtraction assay generated 239 (~80%) unique peptides that were represented by only 1 or 2 colonies (Fig. 3-17, A). From the 118 GFP$^{-/lo}$ unique sequences, three were repeated twice (GGDSADT, RYAVGSK, and TARTGRG) (Fig. 3-17, B and C), and these three peptides will be further investigated, in the near future, to characterize their binding properties (Fig. 3-17). We will also review the GFP$^{-/lo}$ and GFP$^+$ sequences in an effort to identify any motifs that are unique to the PSA$^{-/lo}$ sequences. One reason that could account for the increased number of unique peptides is that in contrast to the indirect subtraction and competitive assays, in the direct subtraction assay incubation of the cells with the phage libraries occurs after FACS, thus bypassing FACS effect of washing loosely bound peptides off.
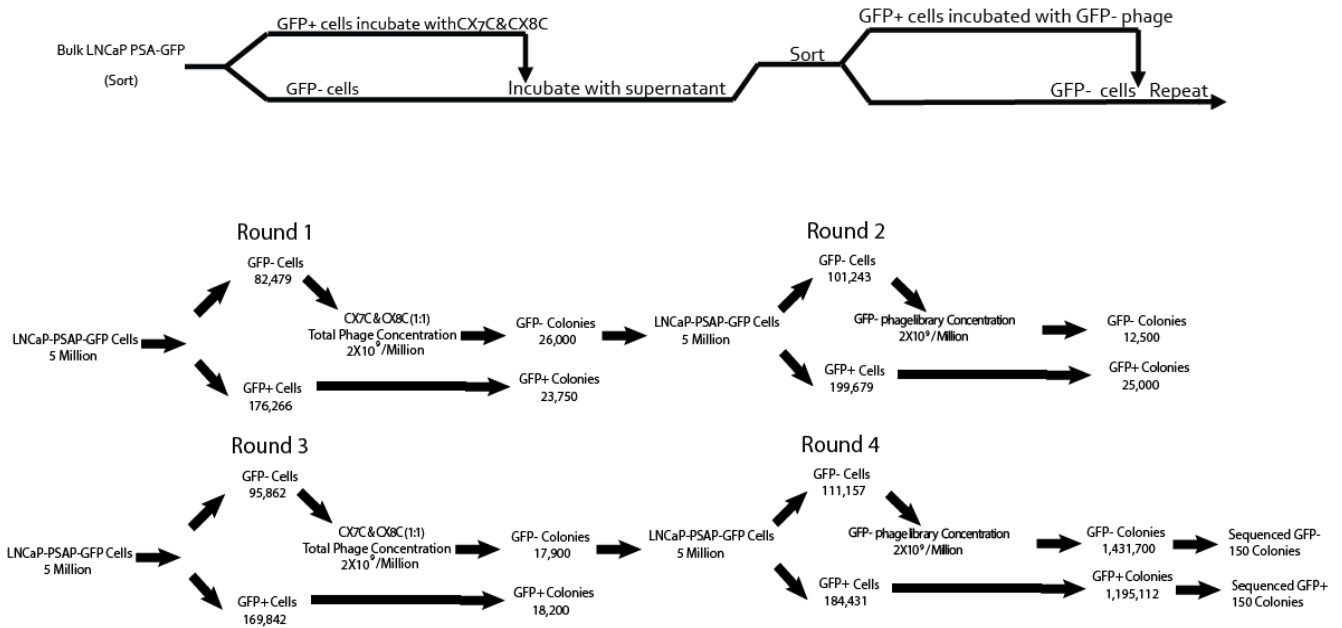
Figure 3-15. Direct subtraction assays used to find unique peptides that bind the PSA$^{-/lo}$ LNCaP cells.

(**A**). Experimental design of direct subtraction assay.

(**B**). Summary of the results from direct subtraction assay, including phage concentrations, cells obtained from FACS, and colonies collected after each round of purification.
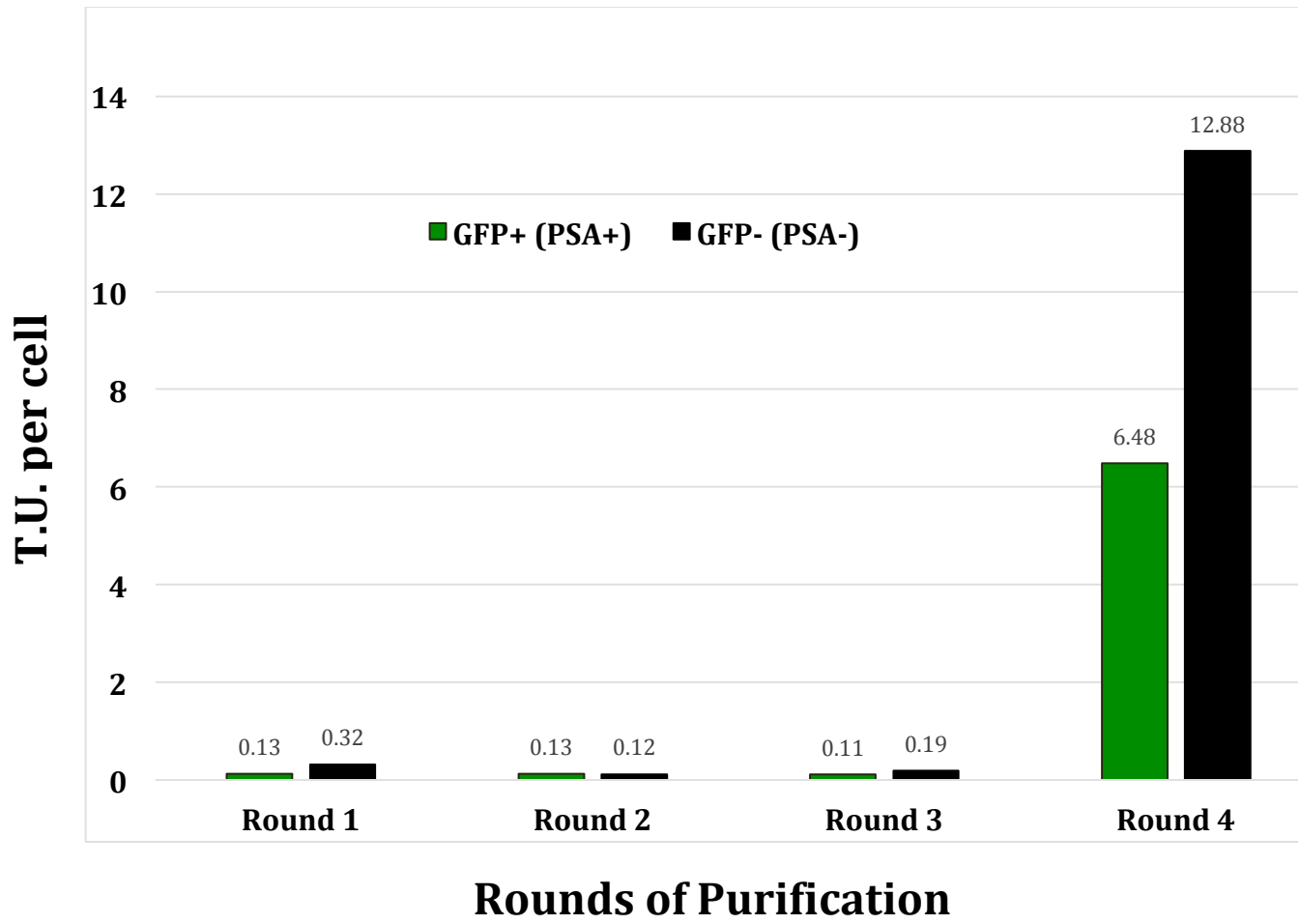
Figure 3-16. Transforming units per cell obtained at each round of purification in the direct subtraction assay. See text for more descriptions

A   Direct Subtraction Results

		Predominant sequences		
Total sequenced=	301	Sequences	GFP-	GFP+
Unreadable sequences=	2	HFWWLEWE	16	15
Negative control=	1	GRAGWYP	10	10
Readable sequences=	298	RLLTDRWG	4	4
Predominant sequences=	59			
GFP- only sequences=	118			
GFP+ only sequences=	121			

B

GFP- repeated sequences

Sequences	Clones
GGDSADT	2
RYAVGSK	2
TARTGRG	2

C   BLAST results for direct subtraction

| Description	Query cover	Max score	Total score	E value	Identity
GGDSADT					
probable ATP-dependent RNA helicase DDXisoform4	100%	18.0	18.0	181	71%
PREDICTED: ras and EF-hand domain-containing protein isoform X2	100%	18.0	18.0	181	71%
RYAVGSK					
Tyrosine-protein phosphatase non-receptor type 21	100%	18.0	18.0	181	71%
PREDICTED: meiosis arrest female protein 1 isoform X6	100%	16.8	16.8	459	71%
TARTGRG					
PREDICTED: phosphatidylinositol 4-kinase alpha isoform X2	100%	19.3	19.3	73	86%
PREDICTED: phosphatidylinositol 4-kinase alpha isoform X1	100%	19.3	19.3	73	86%

Figure 3-17. Direct subtraction assay results

(**A**). List of all of the sequences collected and which group they belong and a list of the three most predominant sequences.

(**B**). List of GFP$^{-/lo}$ repeated peptide sequences.

(**C**). BLAST results for GGDSADT, RYAVGSK and TARTGRG sorted by query coverage.

3.3.6 Preliminary *in vivo* phage display assay

All preceding phage peptide library screenings were conducted in cultured LNCaP cells. One major deficiency with cultured cancer cells is the lack of supporting stromal cells and microenvironment, which are known to be important for tumor development and progression. As a first step towards overcoming this deficiency, we performed a pilot phage display experiment in the LAPC9 xenograft tumor model, which has both PSA$^+$ and PSA$^{-/lo}$ cellular compartments [62]. We first injected infected LAPC9 PSA-GFP cells into the dorsal prostate of male NOD/SCID mice. Once tumors became palpable, we mixed the CX$_7$C and CX$_8$C bacteriophage libraries to a total concentration of 1×10^{11} and injected it (in 50 µl) through the tail vein of a NOD/SCID mouse. The bacteriophage injection was allowed to circulate in the animal for 1 hour, after which the tumor was dissected out, dissociated into single cells, and used in flow sorting of bottom 5% GFP$^{-/lo}$ cells and top 10% GFP$^+$ cells. We isolated the recovered bacteriophages on each cell type and prepared the corresponding bacteriophage libraries. This process was repeated with the GFP$^{-/lo}$ bacteriophage library for multiple rounds (Fig. 3-18).

The GFP$^{-/lo}$ cells only yielded 31 bacterial colonies, and the GFP$^+$ cells yielded 27 bacterial colonies in the initial round. Despite the low numbers, we proceeded to the second round of purification and amplification, to determine if any of these peptides possessed true affinity and specificity for the GFP$^{-/lo}$ cells. The library derived from the initial GFP$^{-/lo}$ cells was utilized and injected into the tail vain of another NOD/SCID mouse bearing a LAPC9 PSA-GFP orthotopic tumor. In this round, both the GFP$^{-/lo}$ cells and the GFP$^+$ cells only yielded 5 bacterial colonies. This round did not show any enrichment in peptides that

preferentially bound to the PSA$^{-/lo}$ LAPC9 cells. It is obvious that more work is needed to optimize the *in vivo* phage display screening in xenograft tumors.
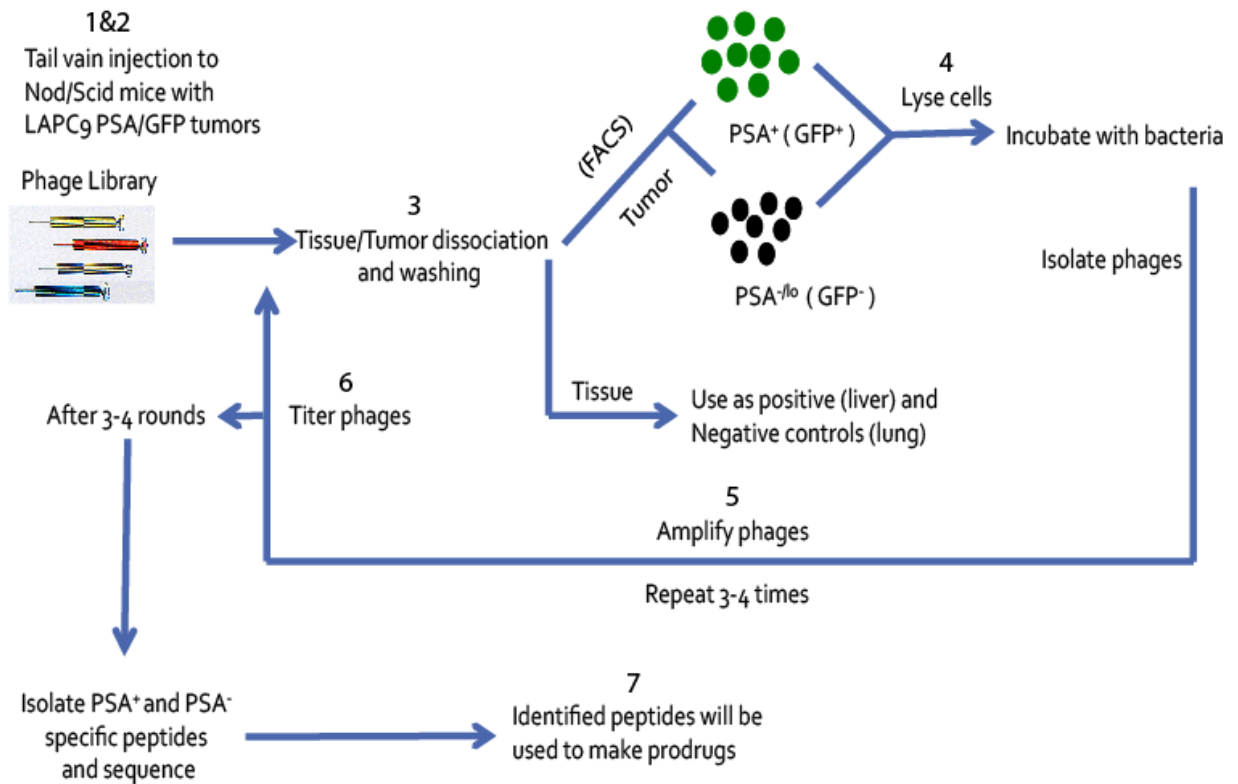
Figure 3-18. Experimental scheme for my *in vivo* phage display screening. Diagram including all relevant steps in my experimental scheme, from the initial injection phage display libraries (CX_7C and CX_8C) (steps 1 and 2), to finally colonies in LB broth and titering the colonies by preforming serial dilutions on K/T plates (steps 5 and 6). Finally, we selected bacterial colonies from each population for sequencing (step 7).

3.4 Discussion

Phage display has been shown to be a powerful tool that has contributed to many different scientific fields. One application of phage display that we are interested in is the design of novel therapeutics that target cancer. By combining rational drug design and peptides that can home into specific PCa cell populations, phage display could lead to the development of novel therapeutics to treat PCa. It could theoretically also be utilized as a diagnostic tool to help identify patients that may be at high risk of relapse. The following studies illustrate the progression from identification of unique peptides, to characterization of a candidate peptide, and finally to the development of drugs conjugated utilizing a peptide.

A key study utilizing phage display was conducted by Arap *et al*. [107], who identified peptides that bound to the human vascular endothelium. In their study, they injected the CX_7C random peptide library into a patient with a B-cell malignancy and after 15 minutes tissue biopsies from various organs (fat, skeletal muscle, bone marrow, skin and prostate) were obtained. Only one round of purification was completed due to ethical concerns. In their study, 47,160 bacteriophages were recovered and sequenced. Analysis of these peptides revealed several motifs and peptides unique to different organ vasculatures. One peptide identified, CGRRAGGSC, may be relevant to PCa. The characterization of this peptide was later shown to specifically bind the α subunit of the interleukin 11 receptor [122]. IL-11 was initially characterized as a cytokine in thrombopoietic activity but later shown to have many different functions in multiple tissues. The CGRRAGGSC peptide induced cell proliferation by activating STAT3, which was inhibited when soluble IL-11Rα was added [122]. These observations suggest that this peptide is a specific IL-11Rα agonist

and may be a good candidate for a pro-drug to prevent chemotherapy-induced thrombocytopenia. Furthermore, PCa cells and the endothelium in PCa have been shown to overexpress IL-11Rα during disease progression, and this peptide is being investigated as a potential drug conjugate to treat PCa [123].

Another study testing the effects of a drug conjugated to a peptide was conducted by Chen *et al.*, who tested a peptide, RGD, which selectively binds to MDA-MB-435 cells derived from a metastatic breast cancer patient [124]. They conjugated this peptide to paclitaxel (PTX), an antimicrotubule agent commonly used to treat advanced metastatic breast cancer. In their study, the peptide-PTX conjugate increased the percentage of cells in G_0/G_1 when compared to cells treated with RGD and PTX (separately) or PTX alone, and it produced more early apoptotic cells than PTX alone [124]. Furthermore, utilizing this pro-drug may reduce the toxicity of PTX and the systemic dose required to obtain antitumor efficacy.

In our phage display studies, we have identified two peptides, JRM1 and JRM2 that demonstrate different levels of preferential binding to the PSA$^{-/lo}$ LNCaP cells, which exhibit many SC characteristics and may represent a cellular source of CRPC. We have also uncovered three new peptides to be characterized using the direct subtraction assay. Finally, we have begun the efforts to identify peptides that show preferential binding to the PSA$^{-/lo}$ cells in LAPC9 tumors using *in vivo* phage display. Our ultimate goal is to identify and further characterize these peptides that can preferentially home in to PSA$^{-/lo}$ PCa cells that show intrinsic resistance to castration.

The first peptide, JRM1, was identified using competitive assays (Fig. 3-2). We characterized this peptide by using multiple methods including synthetic biotinylated JRM1

peptide and having JRM1 directly conjugated to aminocoumarin, and then we quantified its

binding properties to PSA-/lo LNCaP cells by using IF and FACS analysis. These methods

showed relatively consistent results, i.e., a slight preferential binding to the PSA$^{-/lo}$ LNCaP

cells. With these results, we rescreened LNCaP cells using indirect subtraction assays, which

led to the discovery of the peptide JRM2. Then we characterized JRM2 using the same

methods as JRM1 except we additionally conjugated JRM2 to lassamine rhodamine.

Strikingly, JRM2 shows strong preferential binding to the PSA$^{-/lo}$ LNCaP cells utilizing all

methods. As laid out in the 'Future Plan', further characterizing the binding properties and

the utilities of JRM2 represents a top priority for my continued studies. We hope that

ultimately JRM2 can be developed into a PSA$^{-/lo}$ PCa cell specific 'therapeutic' peptide.

We have also identified other peptides using the direct subtraction assays, in which

after FACS, we use the GFP^{+} cells as a sink to eliminate peptides specific to that population

and then use this GFP^{+} peptide depleted library to incubate the GFP$^{-/lo}$ cells. This effort has

resulted in three peptides that are currently being characterized to determine if any of them

truly shows preferential binding to the PSA$^{-/lo}$ PCa cells. Finally, a critical ongoing

experiment is the *in vivo* phage display screening. In this assay, we are utilizing the LAPC9

xenograft model with phage display libraries (Fig. 3-18). We have yet to uncover any

peptides that show increased specificity to the PSA$^{-/lo}$ cells in the LAPC9 tumors. My future

studies will focus on optimizing the protocol.

3.5 Future plan

The use of peptides for targeted delivery of anti-cancer therapeutics has many advantages compared to some other approaches such as monoclonal antibodies. Although monoclonal antibodies may possess high affinity for specific cell surface target molecules, their applications in drug delivery could be limited due to their high molecular weight (150 kDa) and the potential immunogenicity. Peptides, on the other hand, may be more effective due to their relatively lower molecular weight, higher cellular permeability, lower immunogenicity, ease of synthesis, and flexibility in chemical conjugation [125]. For these reasons, further investigation is needed to characterize the already identified peptides and uncover new peptides that show specificity for PSA$^{-/lo}$ PCa cells, which is critical for development of novel therapeutics that target CRPC.

1. <u>More thorough studies of JRM2 peptide binding to PSA$^{-/lo}$ LNCaP cells</u>

A. We will first conduct a dose study by incubating live LNCaP PSA-GFP cells with increasing amounts (i.e, 0, 10, 100, and 200 nM) of JRM2-AMC or JRM2-LR and use FACS analysis and confocal microscopy to determine the percent JRM2 binding to the PSA$^{-/lo}$ LNCaP cells. If the JRM2 peptide specifically binds to the PSA$^{-/lo}$ cells, we expect to observe a dose dependent increase in the percent JRM2 bound PSA$^{-/lo}$ cells.

B. We will determine specificity of JRM2 binding by performing a competition assay. To this end, the LNCaP PSA-GFP cells will be incubated with 200 nM of JRM2-AMC or JRM2-LR, in the presence of increasing unconjugated JRM2. FACS analysis and confocal microscopy will then be performed to evaluate the percent JRM2 binding to the PSA$^{-/lo}$ LNCaP cells. If JRM2 is truly specific, as we increase the amount of unconjugated JRM2,

we will see a gradual decrease in the binding of JRM2-AMC or JRM2-LR to PSA$^{-/lo}$ LNCaP cells.

C.   We will complete a similar dose study as stated in 1-A except LNCaP PSA-GFP cells are fixed in 4% PFA. By using fixed cells, it will eliminate many variables that live cells inherently have because the cell surface molecule that JRM2 is binding to is immobilized, which should give us a more accurate base line of the percent of cells that express JRM2 binding partner. Also, it will give us a pseudo binding affinity profile.

D.   We will determine whether JRM2 also binds to PSA$^{-/lo}$ LNCaP cells *in vivo,* utilizing LNCaP xenograft models in Nod/Scid mice. We will inject 200 nM of JRM2-AMC or JRM2-LR into tail vein of the mouse, let circulate for 1-2 hours, and then dissociate the tumors into single cells and employ FACS and confocal microscopy to analyze JRM2 binding to the PSA$^{-/lo}$ LNCaP cells. This experiment is critical in determining if JRM2 can penetrate the vasculature endothelium and not be degraded in circulation. Also we will collect other organs such as liver and lungs to determine if JRM2 binding is specific to the tumor cells or if JRM2 non-specifically binds to other organs. As an alternative and a backup plan, we may also perform intratumoral injection of the JRM2 peptide.

2. To determine whether JRM2 binds to other PSA$^{-/lo}$ PCa cells utilizing JRM2 AMC and JRM2-LR

First, we will utilize the VCaP cell line, which was developed from a patient with hormone refractory prostate cancer and remains androgen sensitive. We will incubate these cells with JRM2-AMC and JRM2-LR and quantify JRM2's binding properties. We will also utilize LAPC9 cells, which were originally derived from a bone metastasis and have been

maintained as xenograft tumors in Nod/Scid mice. We will inject Nod/Scid mice with JRM2-AMC or JRM2-LR into the tail vein and dissociate the tumors to uncover if JRM2 can bind to the PSA$^{-/lo}$ LAPC9 cells. The prediction is that if the molecule(s) that JRM2 is binding to is shared between LNCaP PSA$^{-/lo}$ and these two cell lines then when we analyze the binding properties of JRM2 we will also see an increase in the binding of JRM2 to the PSA$^{-/lo}$ cells in these two cell lines.

3. To test the utilities of JRM2 by conjugating with cytotoxic peptides or drugs

A.   We will first test if it can be internalized, because it is crucial for the peptide to be internalized when JRM2 is conjugated to a drug or peptide for that drug/peptide to have an effect. To determine if JRM2 peptide can be internalized, I shall plate LNCaP PSA$^{-/lo}$ cells, incubate the cells with JRM2-LR for varying amounts of time, fix the cells, and finally the cells can be permeablized if needed and mounted. If the peptide is internalized then using the confocal microscope we will visualize it inside the cell.

B.   JRM2 will be conjugated with a pro-apoptotic sequence (KLAKLAK)$_2$ [126,127,128]. LNCaP PSA-GFP cells will be sorted into the GFP$^{-/lo}$ and the GFP$^+$ populations and a dose study will be conducted to determine the effect on both populations at increasing doses from 5 nM to 100 nM. Also we will use unsorted LNCaP PSA-GFP cell and perform the same experiment as above to investigate what will happen to the PSA$^{-/lo}$ cells when left with PSA$^+$ cells. We predict that if JRM2 is specific to the PSA$^{-/lo}$ cells then we will see an increase in dead and dying cells in the GFP$^{-/lo}$ wells compared to the GFP$^+$ cells, in the bulk cells we will see a decrease in the GFP$^{-/lo}$ cells. Dr. Kolonin's lab along with others have shown the effectiveness of adding a pro-apoptotic sequence to a peptide to induce cell death.

C.   JRM2 will also be conjugated to a drug to test the cell killing effects. The commonly used drugs for such purposes include methotrexate, 5-fluorouracil, doxorubicin, cyclosporine and paclitaxel [129]. The effects of this JRM2-conjugate can be measured by using LNCaP PSA-GFP cells sorted into the GFP$^{-/lo}$ and the GFP^{+} populations, and a dose study will be conducted to determine the effect on both populations at increasing doses from 5 nM to 100 nM. If JRM2 is specific to the PSA$^{-/lo}$ cells then we will see an increase in dead and dying cells in the GFP$^{-/lo}$ wells compared to the GFP^{+} cells.

4. To characterize the three new peptides recently identified in the direct subtraction assays

We will utilize the same methods as those adopted when characterizing JRM1 and JRM2 peptides.

5. To optimize the protocol for *in vivo* phage display screening utilizing LAPC9 xenograft tumors

Theoretically, the *in vivo* display approach should uncover peptides that will not only be specific to the PSA$^{-/lo}$ LAPC9 cells but will also be able to infiltrate the vasculature. The peptides uncovered in these studies will have the highest likelihood of being therapeutically relevant. So far, we have not been successful at isolating peptides that show preferential binding to the PSA$^{-/lo}$ LAPC9 cells. We shall continue to investigate various parameters based on our experience from multiple *in vitro* assays. As a backup plan, we shall explore the *ex vivo* approach, in which the tumor is excised, dissociated into single cells, and incubated with the phage display library. This method should allow the phages to bypass the vascular barrier and also not be trapped in other organs such as the liver and lung [130].

6. Finally, we will make efforts to determine the potential binding partner(s) of JRM2

One way to acquire indirect evidence for the potential binding partner(s) of JRM2 is to review the BLAST data and to narrow its potential binding partners to a few candidates to see if the PSA$^{-/lo}$ cells overexpress any of the candidates. A direct method of finding JRM2's binding partner is by employing affinity chromatography. Briefly we will extract the membrane proteins from purified PSA$^{-/lo}$ LNCaP cells and apply them to synthetic JRM2 covalently coupled to resin through its C terminus. After the membrane proteins of LNCaP cells are filtered across this resin, specifically bound proteins will then be eluted and subjected to mass spectrometry analysis. The outcome may implicate a pathway that is critical for PCSCs and by uncovering this it could lead to the development of more effective therapeutics against CRPC.

Bibliography

[1] R. Siegel, J. Ma, Z. Zou, A. Jemal. (2014) Cancer statistics, 2014. CA Cancer J Clin 64: 9-29.

[2] M.M. Shen, C. Abate-Shen. (2010) Molecular genetics of prostate cancer: new prospects for old challenges. Genes Dev 24: 1967-2000.

[3] M.F. Clarke, J.E. Dick, P.B. Dirks, C.J. Eaves, C.H. Jamieson, D.L. Jones, J. Visvader, I.L. Weissman, G.M. Wahl. (2006) Cancer stem cells--perspectives on current status and future directions: AACR Workshop on cancer stem cells. Cancer Res 66: 9339-9344.

[4] H. Clevers. (2011) The cancer stem cell: premises, promises and challenges. Nat Med 17: 313-319.

[5] D.G. Tang. (2012) Understanding cancer stem cell heterogeneity and plasticity. Cell Res 22: 457-472.

[6] V.L. Kumar, P.K. Majumder. (1995) Prostate gland: structure, functions and regulation. Int Urol Nephrol 27: 231-243.

[7] P.C. Walsh, Retik, A.B., Stamey, T.A., Vaughan, E.D. (1992) Cambell's Urology. W.B. Saunders Co., Philadelphia.

[8] J.E. McNeal. (1969) Origin and development of carcinoma in the prostate. Cancer 23: 24-34.

[9] J.E. McNeal. (1981) The zonal anatomy of the prostate. Prostate 2: 35-49.

[10] J.E. McNeal. (1988) Normal histology of the prostate. Am J Surg Pathol 12: 619-633.

[11] I.M. Berquin, Y. Min, R. Wu, H. Wu, Y.Q. Chen. (2005) Expression signature of the mouse prostate. J Biol Chem 280: 36442-36451.

[12] D.G. Tang, L. Patrawala, T. Calhoun, B. Bhatia, G. Choy, R. Schneider-Broussard, C. Jeter. (2007) Prostate cancer stem/progenitor cells: identification, characterization, and implications. Mol Carcinog 46: 1-14.

[13] H. Li, D.G. Tang. (2011) Prostate cancer stem cells and their potential roles in metastasis. J Surg Oncol 103: 558-562.

[14] S. Signoretti, D. Waltregny, J. Dilks, B. Isaac, D. Lin, L. Garraway, A. Yang, R. Montironi, F. McKeon, M. Loda. (2000) p63 is a prostate basal cell marker and is required for prostate development. Am J Pathol 157: 1769-1775.

[15] A.Y. Liu, L.D. True, L. LaTray, P.S. Nelson, W.J. Ellis, R.L. Vessella, P.H. Lange, L. Hood, G. van den Engh. (1997) Cell-cell interaction in prostate gene regulation and cytodifferentiation. Proc Natl Acad Sci U S A 94: 10705-10710.

[16] B. Bhatia, S. Tang, P. Yang, A. Doll, G. Aumueller, R.A. Newman, D.G. Tang. (2005) Cell-autonomous induction of functional tumor suppressor 15-lipoxygenase 2 (15-LOX2) contributes to replicative senescence of human prostate progenitor cells. Oncogene 24: 3583-3595.

[17] I.L. Weissman. (2000) Stem cells: units of development, units of regeneration, and units in evolution. Cell 100: 157-168.

[18] H.F. English, R.J. Santen, J.T. Isaacs. (1987) Response of glandular versus basal rat ventral prostatic epithelial cells to androgen withdrawal and replacement. Prostate 11: 229-242.

[19] P.E. Burger, X. Xiong, S. Coetzee, S.N. Salm, D. Moscatelli, K. Goto, E.L. Wilson. (2005) Sca-1 expression identifies stem cells in the proximal region of prostatic ducts with high capacity to reconstitute prostatic tissue. Proc Natl Acad Sci U S A 102: 7180-7185.

[20] D.A. Lawson, L. Xin, R.U. Lukacs, D. Cheng, O.N. Witte. (2007) Isolation and functional characterization of murine prostate stem cells. Proc Natl Acad Sci U S A 104: 181-186.

[21] A.S. Goldstein, D.A. Lawson, D. Cheng, W. Sun, I.P. Garraway, O.N. Witte. (2008) Trop2 identifies a subpopulation of murine and human prostate basal cells with stem cell characteristics. Proc Natl Acad Sci U S A 105: 20882-20887.

[22] K.G. Leong, B.E. Wang, L. Johnson, W.Q. Gao. (2008) Generation of a prostate from a single adult stem cell. Nature 456: 804-808.

[23] T. Kurita, R.T. Medina, A.A. Mills, G.R. Cunha. (2004) Role of p63 and basal cells in the prostate. Development 131: 4955-4964.

[24] X. Wang, M. Kruithof-de Julio, K.D. Economides, D. Walker, H. Yu, M.V. Halili, Y.P. Hu, S.M. Price, C. Abate-Shen, M.M. Shen. (2009) A luminal epithelial stem cell that is a cell of origin for prostate cancer. Nature 461: 495-500.

[25] N. Choi, B. Zhang, L. Zhang, M. Ittmann, L. Xin. (2012) Adult murine prostate basal and luminal cells are self-sustained lineages that can both serve as targets for prostate cancer initiation. Cancer Cell 21: 253-265.

[26] A.T. Collins, F.K. Habib, N.J. Maitland, D.E. Neal. (2001) Identification and isolation of human prostate epithelial stem cells based on alpha(2)beta(1)-integrin expression. J Cell Sci 114: 3865-3872.

85

[27] G.D. Richardson, C.N. Robson, S.H. Lang, D.E. Neal, N.J. Maitland, A.T. Collins. (2004) CD133, a novel marker for human prostatic epithelial stem cells. J Cell Sci 117: 3539-3545.

[28] Q. Wang, W. Li, Y. Zhang, X. Yuan, K. Xu, J. Yu, Z. Chen, R. Beroukhim, H. Wang, M. Lupien, T. Wu, M.M. Regan, C.A. Meyer, J.S. Carroll, A.K. Manrai, O.A. Janne, S.P. Balk, R. Mehra, B. Han, A.M. Chinnaiyan, M.A. Rubin, L. True, M. Fiorentino, C. Fiore, M. Loda, P.W. Kantoff, X.S. Liu, M. Brown. (2009) Androgen receptor regulates a distinct transcription program in androgen-independent prostate cancer. Cell 138: 245-256.

[29] S.A. Tomlins, D.R. Rhodes, S. Perner, S.M. Dhanasekaran, R. Mehra, X.W. Sun, S. Varambally, X. Cao, J. Tchinda, R. Kuefer, C. Lee, J.E. Montie, R.B. Shah, K.J. Pienta, M.A. Rubin, A.M. Chinnaiyan. (2005) Recurrent fusion of TMPRSS2 and ETS transcription factor genes in prostate cancer. Science 310: 644-648.

[30] C. Kumar-Sinha, S.A. Tomlins, A.M. Chinnaiyan. (2008) Recurrent gene fusions in prostate cancer. Nat Rev Cancer 8: 497-511.

[31] B.J. Feldman, D. Feldman. (2001) The development of androgen-independent prostate cancer. Nat Rev Cancer 1: 34-45.

[32] M.R. Cooperberg, J.W. Moul, P.R. Carroll. (2005) The changing face of prostate cancer. J Clin Oncol 23: 8146-8151.

[33] P.C. Nowell. (1976) The clonal evolution of tumor cell populations. Science 194: 23-28.

[34] P.C. Nowell, D.A. Hungerford. (1960) Chromosome studies on normal and leukemic human leukocytes. J Natl Cancer Inst 25: 85-109.

[35] J.E. Visvader, G.J. Lindeman. (2008) Cancer stem cells in solid tumours: accumulating evidence and unresolved questions. Nat Rev Cancer 8: 755-768.

[36] J.a.K. Furth, M. (1937) The transmission of leukemia of mice with a single cell. AM J Cancer 31: 276-282.

[37] T. Lapidot, C. Sirard, J. Vormoor, B. Murdoch, T. Hoang, J. Caceres-Cortes, M. Minden, B. Paterson, M.A. Caligiuri, J.E. Dick. (1994) A cell initiating human acute myeloid leukaemia after transplantation into SCID mice. Nature 367: 645-648.

[38] D. Bonnet, J.E. Dick. (1997) Human acute myeloid leukemia is organized as a hierarchy that originates from a primitive hematopoietic cell. Nat Med 3: 730-737.

[39] M. Al-Hajj, M.S. Wicha, A. Benito-Hernandez, S.J. Morrison, M.F. Clarke. (2003) Prospective identification of tumorigenic breast cancer cells. Proc Natl Acad Sci U S A 100: 3983-3988.

[40] R. Majeti, M.P. Chao, A.A. Alizadeh, W.W. Pang, S. Jaiswal, K.D. Gibbs, Jr., N. van Rooijen, I.L. Weissman. (2009) CD47 is an adverse prognostic factor and therapeutic antibody target on human acute myeloid leukemia stem cells. Cell 138: 286-299.

[41] K. Naka, T. Hoshii, T. Muraguchi, Y. Tadokoro, T. Ooshio, Y. Kondo, S. Nakao, N. Motoyama, A. Hirao. (2010) TGF-beta-FOXO signalling maintains leukaemia-initiating cells in chronic myeloid leukaemia. Nature 463: 676-680.

[42] Y. Wang, A.V. Krivtsov, A.U. Sinha, T.E. North, W. Goessling, Z. Feng, L.I. Zon, S.A. Armstrong. (2010) The Wnt/beta-catenin pathway is required for the development of leukemia stem cells in AML. Science 327: 1650-1653.

[43] F. Notta, C.G. Mullighan, J.C. Wang, A. Poeppl, S. Doulatov, L.A. Phillips, J. Ma, M.D. Minden, J.R. Downing, J.E. Dick. (2011) Evolution of human BCR-ABL1 lymphoblastic leukaemia-initiating cells. Nature 469: 362-367.

[44] F. Yu, H. Yao, P. Zhu, X. Zhang, Q. Pan, C. Gong, Y. Huang, X. Hu, F. Su, J. Lieberman, E. Song. (2007) let-7 regulates self renewal and tumorigenicity of breast cancer cells. Cell 131: 1109-1123.

[45] C. Ginestier, M.H. Hur, E. Charafe-Jauffret, F. Monville, J. Dutcher, M. Brown, J. Jacquemier, P. Viens, C.G. Kleer, S. Liu, A. Schott, D. Hayes, D. Birnbaum, M.S. Wicha, G. Dontu. (2007) ALDH1 is a marker of normal and malignant human mammary stem cells and a predictor of poor clinical outcome. Cell Stem Cell 1: 555-567.

[46] S. Pece, D. Tosoni, S. Confalonieri, G. Mazzarol, M. Vecchi, S. Ronzoni, L. Bernard, G. Viale, P.G. Pelicci, P.P. Di Fiore. (2010) Biological and molecular heterogeneity of breast cancers correlates with their cancer stem cell content. Cell 140: 62-73.

[47] C.A. O'Brien, A. Pollett, S. Gallinger, J.E. Dick. (2007) A human colon cancer cell capable of initiating tumour growth in immunodeficient mice. Nature 445: 106-110.

[48] L. Ricci-Vitiani, D.G. Lombardi, E. Pilozzi, M. Biffoni, M. Todaro, C. Peschle, R. De Maria. (2007) Identification and expansion of human colon-cancer-initiating cells. Nature 445: 111-115.

[49] S.K. Singh, C. Hawkins, I.D. Clarke, J.A. Squire, J. Bayani, T. Hide, R.M. Henkelman, M.D. Cusimano, P.B. Dirks. (2004) Identification of human brain tumour initiating cells. Nature 432: 396-401.

[50] S. Bao, Q. Wu, R.E. McLendon, Y. Hao, Q. Shi, A.B. Hjelmeland, M.W. Dewhirst, D.D. Bigner, J.N. Rich. (2006) Glioma stem cells promote radioresistance by preferential activation of the DNA damage response. Nature 444: 756-760.

[51] C.E. Eyler, Q. Wu, K. Yan, J.M. MacSwords, D. Chandler-Militello, K.L. Misuraca, J.D. Lathia, M.T. Forrester, J. Lee, J.S. Stamler, S.A. Goldman, M. Bredel, R.E. McLendon, A.E. Sloan, A.B. Hjelmeland, J.N. Rich. (2011) Glioma stem cell proliferation and tumor growth are promoted by nitric oxide synthase-2. Cell 146: 53-66.

[52] K.S. Chan, I. Espinosa, M. Chao, D. Wong, L. Ailles, M. Diehn, H. Gill, J. Presti, Jr., H.Y. Chang, M. van de Rijn, L. Shortliffe, I.L. Weissman. (2009) Identification, molecular characterization, clinical prognosis, and therapeutic targeting of human bladder tumor-initiating cells. Proc Natl Acad Sci U S A 106: 14016-14021.

[53] P.L. Ho, E.J. Lay, W. Jian, D. Parra, K.S. Chan. (2012) Stat3 activation in urothelial stem cells leads to direct progression to invasive bladder cancer. Cancer Res 72: 3135-3142.

[54] A. Eramo, F. Lotti, G. Sette, E. Pilozzi, M. Biffoni, A. Di Virgilio, C. Conticello, L. Ruco, C. Peschle, R. De Maria. (2008) Identification and expansion of the tumorigenic lung cancer stem cell population. Cell Death Differ 15: 504-514.

[55] S.J. Curtis, K.W. Sinkevicius, D. Li, A.N. Lau, R.R. Roach, R. Zamponi, A.E. Woolfenden, D.G. Kirsch, K.K. Wong, C.F. Kim. (2010) Primary tumor genotype is an important determinant in identification of lung cancer propagating cells. Cell Stem Cell 7: 127-133.

[56] I.A. Silva, S. Bai, K. McLean, K. Yang, K. Griffith, D. Thomas, C. Ginestier, C. Johnston, A. Kueck, R.K. Reynolds, M.S. Wicha, R.J. Buckanovich. (2011) Aldehyde dehydrogenase in combination with CD133 defines angiogenic ovarian cancer stem cells that portend poor patient survival. Cancer Res 71: 3991-4001.

[57] K. Meirelles, L.A. Benedict, D. Dombkowski, D. Pepin, F.I. Preffer, J. Teixeira, P.S. Tanwar, R.H. Young, D.T. MacLaughlin, P.K. Donahoe, X. Wei. (2012) Human ovarian cancer stem/progenitor cells are stimulated by doxorubicin but inhibited by Mullerian inhibiting substance. Proc Natl Acad Sci U S A 109: 2358-2363.

[58] H. Li, X. Chen, T. Calhoun-Davis, K. Claypool, D.G. Tang. (2008) PC3 human prostate carcinoma cell holoclones contain self-renewing tumor-initiating cells. Cancer Res 68: 1820-1825.

[59] H. Li, M. Jiang, S. Honorio, L. Patrawala, C.R. Jeter, T. Calhoun-Davis, S.W. Hayward, D.G. Tang. (2009) Methodologies in assaying prostate cancer stem cells. Methods Mol Biol 568: 85-138.

[60] C.R. Jeter, M. Badeaux, G. Choy, D. Chandra, L. Patrawala, C. Liu, T. Calhoun-Davis, H. Zaehres, G.Q. Daley, D.G. Tang. (2009) Functional evidence that the self-renewal gene NANOG regulates human tumor development. Stem Cells 27: 993-1005.

[61] C.R. Jeter, B. Liu, X. Liu, X. Chen, C. Liu, T. Calhoun-Davis, J. Repass, H. Zaehres, J.J. Shen, D.G. Tang. (2011) NANOG promotes cancer stem cell characteristics and prostate cancer resistance to androgen deprivation. Oncogene 30: 3833-3845.

[62] J. Qin, X. Liu, B. Laffin, X. Chen, G. Choy, C.R. Jeter, T. Calhoun-Davis, H. Li, G.S. Palapattu, S. Pang, K. Lin, J. Huang, I. Ivanov, W. Li, M.V. Suraneni, D.G. Tang.

(2012) The PSA(-/lo) prostate cancer cell population harbors self-renewing long-term tumor-propagating cells that resist castration. Cell Stem Cell 10: 556-569.

[63] J. Allison, Y.L. Zhang, M.G. Parker. (1989) Tissue-specific and hormonal regulation of the gene for rat prostatic steroid-binding protein in transgenic mice. Mol Cell Biol 9: 2254-2257.

[64] I.G. Maroulakou, M. Anver, L. Garrett, J.E. Green. (1994) Prostate and mammary adenocarcinoma in transgenic mice carrying a rat C3(1) simian virus 40 large tumor antigen fusion gene. Proc Natl Acad Sci U S A 91: 11236-11240.

[65] X. Zhang, M.W. Chen, A. Ng, P.Y. Ng, C. Lee, M. Rubin, C.A. Olsson, R. Buttyan. (1997) Abnormal prostate development in C3(1)-bcl-2 transgenic mice. Prostate 32: 16-26.

[66] X. Zhang, C. Lee, P.Y. Ng, M. Rubin, A. Shabsigh, R. Buttyan. (2000) Prostatic neoplasia in transgenic mice with prostate-directed overexpression of the c-myc oncoprotein. Prostate 43: 278-285.

[67] M. Parisotto, D. Metzger. (2013) Genetically engineered mouse models of prostate cancer. Mol Oncol 7: 190-205.

[68] N.M. Greenberg, F. DeMayo, M.J. Finegold, D. Medina, W.D. Tilley, J.O. Aspinall, G.R. Cunha, A.A. Donjacour, R.J. Matusik, J.M. Rosen. (1995) Prostate cancer in a transgenic mouse. Proc Natl Acad Sci U S A 92: 3439-3443.

[69] Y. Yan, P.C. Sheppard, S. Kasper, L. Lin, S. Hoare, A. Kapoor, J.G. Dodd, M.L. Duckworth, R.J. Matusik. (1997) Large fragment of the probasin promoter targets high levels of transgene expression to the prostate of transgenic mice. Prostate 32: 129-139.

[70] X. Wu, J. Wu, J. Huang, W.C. Powell, J. Zhang, R.J. Matusik, F.O. Sangiorgi, R.E. Maxson, H.M. Sucov, P. Roy-Burman. (2001) Generation of a prostate epithelial cell-specific Cre transgenic mouse model for tissue-specific gene ablation. Mech Dev 101: 61-69.

[71] J. Zhang, T.Z. Thomas, S. Kasper, R.J. Matusik. (2000) A small composite probasin promoter confers high levels of prostate-specific gene expression through regulation by androgens and glucocorticoids in vitro and in vivo. Endocrinology 141: 4698-4710.

[72] J.R. Gingrich, R.J. Barrios, R.A. Morton, B.F. Boyce, F.J. DeMayo, M.J. Finegold, R. Angelopoulou, J.M. Rosen, N.M. Greenberg. (1996) Metastatic prostate cancer in a transgenic mouse. Cancer Res 56: 4096-4102.

[73] P.J. Kaplan-Lefko, T.M. Chen, M.M. Ittmann, R.J. Barrios, G.E. Ayala, W.J. Huss, L.A. Maddison, B.A. Foster, N.M. Greenberg. (2003) Pathobiology of autochthonous prostate cancer in a pre-clinical transgenic mouse model. Prostate 55: 219-237.

[74] K. Sato, J. Qian, J.M. Slezak, M.M. Lieber, D.G. Bostwick, E.J. Bergstralh, R.B. Jenkins. (1999) Clinical significance of alterations of chromosome 8 in high-grade, advanced, nonmetastatic prostate carcinoma. J Natl Cancer Inst 91: 1574-1580.

[75] J. Qian, R.B. Jenkins, D.G. Bostwick. (1997) Detection of chromosomal anomalies and c-myc gene amplification in the cribriform pattern of prostatic intraepithelial neoplasia and carcinoma by fluorescence in situ hybridization. Mod Pathol 10: 1113-1119.

[76] C.E. Nesbit, J.M. Tersak, E.V. Prochownik. (1999) MYC oncogenes and human neoplastic disease. Oncogene 18: 3004-3016.

[77] R.B. Jenkins, J. Qian, M.M. Lieber, D.G. Bostwick. (1997) Detection of c-myc oncogene amplification and chromosomal anomalies in metastatic prostatic carcinoma by fluorescence in situ hybridization. Cancer Res 57: 524-531.

[78] W.H. Fleming, A. Hamel, R. MacDonald, E. Ramsey, N.M. Pettigrew, B. Johnston, J.G. Dodd, R.J. Matusik. (1986) Expression of the c-myc protooncogene in human prostatic carcinoma and benign prostatic hyperplasia. Cancer Res 46: 1535-1538.

[79] K. Ellwood-Yen, T.G. Graeber, J. Wongvipat, M.L. Iruela-Arispe, J. Zhang, R. Matusik, G.V. Thomas, C.L. Sawyers. (2003) Myc-driven murine prostate cancer shares molecular features with human prostate tumors. Cancer Cell 4: 223-238.

[80] M.R. Capecchi. (1994) Targeted gene replacement. Sci Am 270: 52-59.

[81] A. Di Cristofano, B. Pesce, C. Cordon-Cardo, P.P. Pandolfi. (1998) Pten is essential for embryonic development and tumour suppression. Nat Genet 19: 348-355.

[82] K. Podsypanina, L.H. Ellenson, A. Nemes, J. Gu, M. Tamura, K.M. Yamada, C. Cordon-Cardo, G. Catoretti, P.E. Fisher, R. Parsons. (1999) Mutation of Pten/Mmac1 in mice causes neoplasia in multiple organ systems. Proc Natl Acad Sci U S A 96: 1563-1568.

[83] V. Stambolic, M.S. Tsao, D. Macpherson, A. Suzuki, W.B. Chapman, T.W. Mak. (2000) High incidence of breast and endometrial neoplasia resembling human Cowden syndrome in pten+/- mice. Cancer Res 60: 3605-3611.

[84] A. Suzuki, J.L. de la Pompa, V. Stambolic, A.J. Elia, T. Sasaki, I. del Barco Barrantes, A. Ho, A. Wakeham, A. Itie, W. Khoo, M. Fukumoto, T.W. Mak. (1998) High cancer susceptibility and embryonic lethality associated with mutation of the PTEN tumor suppressor gene in mice. Curr Biol 8: 1169-1178.

[85] M.J. You, D.H. Castrillon, B.C. Bastian, R.C. O'Hagan, M.W. Bosenberg, R. Parsons, L. Chin, R.A. DePinho. (2002) Genetic analysis of Pten and Ink4a/Arf interactions in the suppression of tumorigenesis in mice. Proc Natl Acad Sci U S A 99: 1455-1460.

[86] Z. Chen, L.C. Trotman, D. Shaffer, H.K. Lin, Z.A. Dotan, M. Niki, J.A. Koutcher, H.I. Scher, T. Ludwig, W. Gerald, C. Cordon-Cardo, P.P. Pandolfi. (2005) Crucial role of p53-dependent cellular senescence in suppression of Pten-deficient tumorigenesis. Nature 436: 725-730.

[87] M.V. Suraneni, R. Schneider-Broussard, J.R. Moore, T.C. Davis, C.J. Maldonado, H. Li, R.A. Newman, D. Kusewitt, J. Hu, P. Yang, D.G. Tang. (2010) Transgenic expression of 15-lipoxygenase 2 (15-LOX2) in mouse prostate leads to hyperplasia and cell senescence. Oncogene 29: 4261-4275.

[88] G.P. Smith. (1985) Filamentous fusion phage: novel expression vectors that display cloned antigens on the virion surface. Science 228: 1315-1317.

[89] R. Schier, A. McCall, G.P. Adams, K.W. Marshall, H. Merritt, M. Yim, R.S. Crawford, L.M. Weiner, C. Marks, J.D. Marks. (1996) Isolation of picomolar affinity anti-c-erbB-2 single-chain Fv by molecular evolution of the complementarity determining regions in the center of the antibody binding site. J Mol Biol 263: 551-567.

[90] w.w.N.a.C. Inc, Molecular Biology of Viruses, in: S. Foster (Ed.), Microbiology, 2010.

[91] W.W. Ja, R.W. Roberts. (2005) G-protein-directed ligand discovery with peptide combinatorial libraries. Trends Biochem Sci 30: 318-324.

[92] N.C. Wrighton, F.X. Farrell, R. Chang, A.K. Kashyap, F.P. Barbone, L.S. Mulcahy, D.L. Johnson, R.W. Barrett, L.K. Jolliffe, W.J. Dower. (1996) Small peptides as potent mimetics of the protein hormone erythropoietin. Science 273: 458-464.

[93] S.E. Cwirla, P. Balasubramanian, D.J. Duffin, C.R. Wagstrom, C.M. Gates, S.C. Singer, A.M. Davis, R.L. Tansik, L.C. Mattheakis, C.M. Boytos, P.J. Schatz, D.P. Baccanari, N.C. Wrighton, R.W. Barrett, W.J. Dower. (1997) Peptide agonist of the thrombopoietin receptor as potent as the natural cytokine. Science 276: 1696-1699.

[94] J.L. Su, K.P. Lai, C.A. Chen, C.Y. Yang, P.S. Chen, C.C. Chang, C.H. Chou, C.L. Hu, M.L. Kuo, C.Y. Hsieh, L.H. Wei. (2005) A novel peptide specifically binding to interleukin-6 receptor (gp80) inhibits angiogenesis and tumor growth. Cancer Res 65: 4827-4835.

[95] L. Hetian, A. Ping, S. Shumei, L. Xiaoying, H. Luowen, W. Jian, M. Lin, L. Meisheng, Y. Junshan, S. Chengchao. (2002) A novel peptide isolated from a phage display library inhibits tumor growth and metastasis by blocking the binding of vascular endothelial growth factor to its kinase domain receptor. J Biol Chem 277: 43137-43142.

[96] H. Schooltink, S. Rose-John. (2005) Designing cytokine variants by phage-display. Comb Chem High Throughput Screen 8: 173-179.

[97] S.J. McConnell, T. Dinh, M.H. Le, S.J. Brown, K. Becherer, K. Blumeyer, C. Kautzer, F. Axelrod, D.G. Spinella. (1998) Isolation of erythropoietin receptor agonist peptides using evolved phage libraries. Biol Chem 379: 1279-1286.

[98] M.E. Tipps, J.E. Lawshe, A.D. Ellington, S.J. Mihic. (2010) Identification of novel specific allosteric modulators of the glycine receptor using phage display. J Biol Chem 285: 22840-22845.

[99] J. Tao, P. Wendler, G. Connelly, A. Lim, J. Zhang, M. King, T. Li, J.A. Silverman, P.R. Schimmel, F.P. Tally. (2000) Drug target validation: lethal infection blocked by inducible peptide. Proc Natl Acad Sci U S A 97: 783-786.

[100] H.Y. Hong, H.Y. Lee, W. Kwak, J. Yoo, M.H. Na, I.S. So, T.H. Kwon, H.S. Park, S. Huh, G.T. Oh, I.C. Kwon, I.S. Kim, B.H. Lee. (2008) Phage display selection of peptides that home to atherosclerotic plaques: IL-4 receptor as a candidate target in atherosclerosis. J Cell Mol Med 12: 2003-2014.

[101] R. Sedlacek, E. Chen. (2005) Screening for protease substrate by polyvalent phage display. Comb Chem High Throughput Screen 8: 197-203.

[102] B.K. Kay, P.T. Hamilton. (2001) Identification of enzyme inhibitors from phage-displayed combinatorial peptide libraries. Comb Chem High Throughput Screen 4: 535-543.

[103] M.J. Rowley, K. O'Connor, L. Wijeyewickrema. (2004) Phage display for epitope determination: a paradigm for identifying receptor-ligand interactions. Biotechnol Annu Rev 10: 151-188.

[104] A. Skerra. (2007) Alternative non-antibody scaffolds for molecular recognition. Curr Opin Biotechnol 18: 295-304.

[105] C. Gronwall, S. Stahl. (2009) Engineered affinity proteins--generation and applications. J Biotechnol 140: 254-269.

[106] A. Sergeeva, M.G. Kolonin, J.J. Molldrem, R. Pasqualini, W. Arap. (2006) Display technologies: application for the discovery of drug and gene delivery agents. Adv Drug Deliv Rev 58: 1622-1654.

[107] W. Arap, M.G. Kolonin, M. Trepel, J. Lahdenranta, M. Cardo-Vila, R.J. Giordano, P.J. Mintz, P.U. Ardelt, V.J. Yao, C.I. Vidal, L. Chen, A. Flamm, H. Valtanen, L.M. Weavind, M.E. Hicks, R.E. Pollock, G.H. Botz, C.D. Bucana, E. Koivunen, D. Cahill, P. Troncoso, K.A. Baggerly, R.D. Pentz, K.A. Do, C.J. Logothetis, R. Pasqualini.

(2002) Steps toward mapping the human vasculature by phage display. Nat Med 8: 121-127.

[108] S.M. Lee, E.J. Lee, H.Y. Hong, M.K. Kwon, T.H. Kwon, J.Y. Choi, R.W. Park, T.G. Kwon, E.S. Yoo, G.S. Yoon, I.S. Kim, E. Ruoslahti, B.H. Lee. (2007) Targeting bladder tumor cells in vivo and in the urine with a peptide identified by phage display. Mol Cancer Res 5: 11-19.

[109] X. Zhu, H. Wu, S. Luo, Z. Xianyu, D. Zhu. (2008) Screening and identification of a novel hepatocellular carcinoma cell binding peptide by using a phage display library. J Huazhong Univ Sci Technolog Med Sci 28: 299-303.

[110] P. Laakkonen, K. Porkka, J.A. Hoffman, E. Ruoslahti. (2002) A tumor-homing peptide with a targeting specificity related to lymphatic vessels. Nat Med 8: 751-755.

[111] H. Witt, K. Hajdin, K. Iljin, O. Greiner, F.K. Niggli, B.W. Schafer, M. Bernasconi. (2009) Identification of a rhabdomyosarcoma targeting peptide by phage display with sequence similarities to the tumour lymphatic-homing peptide LyP-1. Int J Cancer 124: 2026-2032.

[112] B. Zhang, Y. Zhang, J. Wang, Y. Zhang, J. Chen, Y. Pan, L. Ren, Z. Hu, J. Zhao, M. Liao, S. Wang. (2007) Screening and identification of a targeting peptide to hepatocarcinoma from a phage display peptide library. Mol Med 13: 246-254.

[113] R.J. Giordano, M. Cardo-Vila, J. Lahdenranta, R. Pasqualini, W. Arap. (2001) Biopanning and rapid analysis of selective interactive ligands. Nat Med 7: 1249-1253.

[114] R.J. Giordano, C.D. Anobom, M. Cardo-Vila, J. Kalil, A.P. Valente, R. Pasqualini, F.C. Almeida, W. Arap. (2005) Structural basis for the interaction of a vascular

endothelial growth factor mimic peptide motif and its corresponding receptors. Chem Biol 12: 1075-1083.

[115] A.C. Daquinag, Y. Zhang, F. Amaya-Manzanares, P.J. Simmons, M.G. Kolonin. (2011) An isoform of decorin is a resistin receptor on the surface of adipose progenitor cells. Cell Stem Cell 9: 74-86.

[116] L.S. Jespers, A. Roberts, S.M. Mahler, G. Winter, H.R. Hoogenboom. (1994) Guiding the selection of human antibodies from phage display repertoires to a single epitope of an antigen. Biotechnology (N Y) 12: 899-903.

[117] J.H. Levy, P.S. O'Donnell. (2006) The therapeutic potential of a kallikrein inhibitor for treating hereditary angioedema. Expert Opin Investig Drugs 15: 1077-1090.

[118] S.P. Balk, Y.J. Ko, G.J. Bubley. (2003) Biology of prostate-specific antigen. J Clin Oncol 21: 383-391.

[119] D. Yu, D. Chen, C. Chiu, B. Razmazma, Y.H. Chow, S. Pang. (2001) Prostate-specific targeting using PSA promoter-based lentiviral vectors. Cancer Gene Ther 8: 628-635.

[120] M.G. Kolonin, J. Sun, K.A. Do, C.I. Vidal, Y. Ji, K.A. Baggerly, R. Pasqualini, W. Arap. (2006) Synchronous selection of homing peptides for multiple tissues by in vivo phage display. FASEB J 20: 979-981.

[121] Y. Zhang, A. Daquinag, D.O. Traktuev, F. Amaya-Manzanares, P.J. Simmons, K.L. March, R. Pasqualini, W. Arap, M.G. Kolonin. (2009) White adipose tissue cells are recruited by experimental tumors and promote cancer progression in mouse models. Cancer Res 69: 5259-5266.

[122] M. Cardo-Vila, A.J. Zurita, R.J. Giordano, J. Sun, R. Rangel, L. Guzman-Rojas, C.D. Anobom, A.P. Valente, F.C. Almeida, J. Lahdenranta, M.G. Kolonin, W. Arap, R.

Pasqualini. (2008) A ligand peptide motif selected from a cancer patient is a receptor-interacting site within human interleukin-11. PLoS One 3: e3452.

[123] A.J. Zurita, P. Troncoso, M. Cardo-Vila, C.J. Logothetis, R. Pasqualini, W. Arap. (2004) Combinatorial screenings in patients: the interleukin-11 receptor alpha as a candidate target in the progression of human prostate cancer. Cancer Res 64: 435-439.

[124] X. Chen, C. Plasencia, Y. Hou, N. Neamati. (2005) Synthesis and biological evaluation of dimeric RGD peptide-paclitaxel conjugate as a model for integrin-targeted drug delivery. Journal of medicinal chemistry 48: 1098-1106.

[125] W. Tai, R. Mahato, K. Cheng. (2010) The role of HER2 in cancer therapy and targeted drug delivery. J Control Release 146: 264-275.

[126] M.M. Javadpour, M.M. Juban, W.C. Lo, S.M. Bishop, J.B. Alberty, S.M. Cowell, C.L. Becker, M.L. McLaughlin. (1996) De novo antimicrobial peptides with low mammalian cell toxicity. Journal of medicinal chemistry 39: 3107-3113.

[127] H.M. Ellerby, W. Arap, L.M. Ellerby, R. Kain, R. Andrusiak, G.D. Rio, S. Krajewski, C.R. Lombardo, R. Rao, E. Ruoslahti, D.E. Bredesen, R. Pasqualini. (1999) Anti-cancer activity of targeted pro-apoptotic peptides. Nat Med 5: 1032-1038.

[128] M.G. Kolonin, P.K. Saha, L. Chan, R. Pasqualini, W. Arap. (2004) Reversal of obesity by targeted ablation of adipose tissue. Nat Med 10: 625-632.

[129] K.M. Stewart, K.L. Horton, S.O. Kelley. (2008) Cell-penetrating peptides as delivery vehicles for biology and medicine. Organic & biomolecular chemistry 6: 2242-2255.

[130] J.A.L. Hoffman, P.; Porkka, K.; Bernasconi, M.; Ruoslahti, E. (2004) In vivo and ex vivo selections using phage-displayed libraries. In Phage Display: A Practical Approach. Oxford University Press, New York, NY, USA.

VITA

John Robert Moore was born in Fort Worth Texas on July, 16 1981, the son of Dwaine and Lou Ann Moore. After graduating from Midland Christian High School in 2000, he entered Texas A&M University. John earned the degree of Bachelor of Science in December of 2005. In 2008, he began working in Dr. Dean G. Tang's lab as a research assistant. In the Fall of 2011, John entered The University of Texas Health Science Center at Houston Graduate School of Biomedical Sciences (GSBS) to pursue his Master's degree under the mentorship of Dr. Dean G. Tang.

Permanent address:

321 Cottle Town Rd

Smithville, TX 78957